Journal Pre-proof

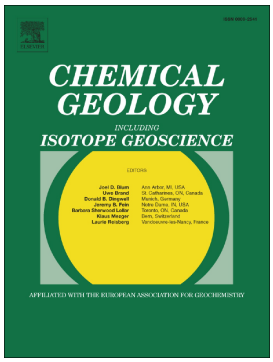

Flux modulated volcanic-style and magmatic architecture of the Chaxas Volcanic Complex, N. Chile constrained by zircon petrochronology

Charles Lewis, Shanaka de Silva

PII: S0009-2541(26)00214-7

DOI: https://doi.org/10.1016/j.chemgeo.2026.123445

Reference: CHEMGE 123445

To appear in: *Chemical Geology*

Received date: 29 October 2025

Revised date: 17 April 2026

Accepted date: 20 April 2026

Please cite this article as: C. Lewis and S. de Silva, Flux modulated volcanic-style and magmatic architecture of the Chaxas Volcanic Complex, N. Chile constrained by zircon petrochronology, *Chemical Geology* (2024), https://doi.org/10.1016/j.chemgeo.2026.123445

Flux Modulated Volcanic-Style and Magmatic Architecture of the Chaxas Volcanic Complex, N. Chile Constrained by Zircon Petrochronology

Charles Lewis[1†], Shanaka de Silva[2]

[1]Nuclear and Radiochemistry Group, Chemistry Division, Los Alamos National Laboratory, Los Alamos, NM 87545, USA

[2]Oregon State University; College of Earth, Ocean, and Atmospheric Sciences (CEOAS); 104 CEOAS Admin Bldg. Corvallis, OR 97331

[†] Corresponding Author

Abstract

Zircon petrochronology of the Chaxas Volcanic Complex (N. Chile) reveals dynamic intrusive flux with a corresponding volcanic history that parallels pulses of the regional Altiplano-Puna Volcanic Complex (APVC) flare-up. Two distinct stages of eruptive style and flux are recognized. The Pre-Chaxas stage is comprised of silicic ignimbrites, including the 500 km^3 Puripicar Ignimbrite. Pre-Chaxas U-Pb crystallization ages have long durations (Δt) of 1.3 – 4.1 myr due to efficient cannibalization. Autocrystic subpopulations indicate maximum crystallization durations prior to eruption (Δt_Y) of 440 – 950 kyr. Zr/Hf in zircon is partially decoupled from typical proxies for fractionation (e.g., U/Th) and instead track assimilation. Modeled synthetic zircon ages benchmarked by observed zircon ages predict that Pre-Chaxas flux is consistent with flux requirements necessary for supereruptions at 1.2×10^{-4} – 2.3×10^{-4} $km^3\ yr^{-1}\ km^{-2}$. An intrusive volume of ~ 5800 km^3 is estimated for the Pre-Chaxas stage. The younger Chaxas Complex stage consists dominantly of a distributed dacitic dome complex. Δt_Y is shorter relative to the Pre-Chaxas stage and zircon is less efficiently cannibalized. Predicted flux during this stage is nearly an order of magnitude lower ($< 3.2 \times 10^{-5}$ – 5.6×10^{-5} $km^3\ yr^{-1}\ km^{-2}$), with an estimated intrusive volume of 790 km^3. This petrochronologic record shows that volcanic style and subvolcanic architecture are sensitive to variations in magmatic flux, shifting by an order of magnitude over only a few hundred kyr.

Introduction

The tempo of volcanic activity and the assembly of upper crustal reservoirs beneath continental volcanic arcs is heavily dependent on the duration of magmatic activity and attendant flux (Hildreth, 1981). Flux can be described as a spectrum of two endmembers where magmatic systems can be characterized by a low flux regime that produces ephemeral melt batches, or a more vigorous, high flux regime that promotes large volumes of eruptible magma (Tavazzani et al., 2023). Suprasolidus durations of small intrusions produced during low flux are thought to have maximum residence times down to 10's of kyr (Barboni et al., 2015; Pamukçu et al., 2025) whereas larger and incrementally grown magmatic systems may show melt residence for 100's of kyr or even up to 1 myr prior to eruption (Curry et al., 2021; Kaiser et al., 2017). While numerous empirical examples of both flux regimes have been described (c.f., Angeles-De La Torre et al., 2023; Curry et al., 2021; Kaiser et al., 2017a; Rivera et al., 2016; Samperton et al., 2017), there are few studies that quantify the magnitude of changes in flux within long-lived systems and how quickly these changes may occur.

Regional ignimbrite flare-ups record Earth's most prodigious periods of magmatism (Coney and Reynolds, 1977) producing tens of thousands of cubic kilometers of magma erupted during volcanic fluxes ranging from $10^1 – 10^3$ km^3 kyr^{-1} (Bertin et al., 2023; Best et al., 2016). The volcanic record of such flare-ups often consists of extensive ignimbrites emanating from polycyclic caldera clusters. With volumes of $10^2 – 10^3$ km^3, these ignimbrites have been demonstrated to represent the evacuation of the tops of extensive upper crustal plutonic complexes (Best et al., 2016; Lipman et al., 1978). Resolving the spatiotemporal organization of such large silicic reservoirs is necessary for describing the assembly of granitic batholiths and the pre-eruptive build-up within magmatic systems that produce Earth's largest eruptions. Many flare-up related volcanic systems also have extensive lifecycles that record dramatic changes in volcanic flux that is intricately linked to eruptive style (Angeles-De La Torre et al., 2023; Burns et al., 2015; Grunder et al., 2006). Quantifying the variation of magmatic flux within such systems may provide constraints on the maturation of continental magmatic arcs that produce chronologically and geochemically complex granitic batholiths (e.g., Matzel et al., 2006).

Secular changes within magmatic systems can be resolved through combined geochronology and petrology ("petro-chronology") by analyzing mineral phases that strongly partition radiogenic parents while excluding daughter elements (Schmitt and Vazquez, 2017; Tavazzani et al., 2023). Zircon specifically serves as a robust U-Pb petrochronologic tool due to its resistance to chemical alteration, predictable and early saturation within silicic magmas, and ability to temporally track changes in magma temperature and chemistry. In idealized and some

natural cases zircon petrochronologic studies show magmatic systems have predictable monotonic cooling trends prior to evacuation of ignimbrites and during assembly of plutonic complexes (Samperton et al., 2017; Tappa et al., 2011). In other cases, such petrochronologic studies may record a complex and prolonged thermal history spanning up to 10 myr prior to climactic eruptions (Eddy et al., 2022; Matzel et al., 2006; Tavazzani et al., 2020; Walker et al., 2010). As a result of the capability for U-Pb zircon petrochronology to record such a range of timescales, the approach provides some verisimilitude when used to test the flux regime that produced a volcanic system. One powerful tool to implement this test is the creation of synthetic zircon distributions via thermal modeling to facilitate quantification of the flux which produced observed age distributions (Caricchi et al., 2014; Schmitt et al., 2023; Tierney et. al., 2016). Such an approach leverages empirical observation of U-Pb crystallization histories in volcanic rocks with thermal modeling to test if variation of magmatic fluxes beneath volcanic systems controls volcanic characteristics and eruptive histories (Farina et al., 2024).

Two compositionally equivalent but stylistically distinct volcanic stages have been previously recorded at the Chaxas Volcanic Complex located within the Altiplano Puna Volcanic Complex (APVC) of the Central Andes (Northern Chile) (Lewis et al., 2025). Eruption styles range from the ≥ 500 km^3 Puripicar Ignimbrite dacitic supereruption to effusive dome eruptions and associated block and ash flows during the final stages of magmatism. U-Pb zircon petrochronology from the Chaxas Volcanic Complex presented here tests if the dramatic change in eruptive history is modulated by changes in the magmatic flux regime. Results are then evaluated within the context that ignimbrite flare-up magmatism may have a significant effect on the maturation and construction continental magmatic arcs.

Continental Magmatic Arc Context

Altiplano-Puna Volcanic Complex (APVC)

The ~ 10 – 1 Ma APVC is a 70,000 km^2 region located at the transition between the Altiplano to Puna segments of the Central Andean Plateau of northern Chile that is inundated with ignimbrites. Ignimbrites are dominantly high-K dacites and subordinate rhyolites with crustal radiogenic isotope ratios that are sourced from large caldera structures, nine of which have dense rock equivalent (DRE) volumes of ≥ 430 km^3 (Kern et al., 2016; Salisbury et al., 2011) and are thus categorized as supereruptions (Magnitude (*M*) 8; e.g. de Silva and Self, 2022). The magmas that erupted during the APVC flare-up are the result of extensive assimilation-fractional crystallization that occurs during advection of subduction-related basaltic parental magmas through 70 to 80 km thick sub-Andean crust (Burns and de Silva, 2023; Kay et al., 2010). The

APVC is underlain by the Altiplano-Puna Magma Body (APMB), a seismic low-velocity zone extending from 15-30 km depth that is interpreted as ~ 500,000 km^3 of magma with approximately 20% partial melt (Pritchard et al., 2018; Ward et al., 2014). The APMB has been interpreted to be the andesitic parental reservoir to the 8 to 2 km deep dacitic magma bodies which source the APVC's voluminous ignimbrite eruptions (Grocke et al., 2017; Kaiser et al., 2017b). Volcanic output during the flare-up imply remarkable magma addition rates of ~ 70 km^3 / km arc (parallel to trench) / million years (de Silva and Kay, 2018; Bertin, 2023); substantially higher than the steady state estimate of 20 km^3 / km arc / myr (Jicha and Jagoutz, 2015). The most prolific periods of APVC volcanic activity occurred in fractal pulses, defined as geologically brief timespans of high volcanic output, at 8 ± 1 Ma, 6 ± 1 Ma, 4 ± 1Ma, and 2 ± 1 Ma due to crustal modulation of advecting magmas into and from the APMB (de Silva et al., 2015; Kern et al., 2016).

Chaxas Volcanic Complex Eruptive History and Stratigraphy

The location of the magmatic system beneath the Chaxas Volcanic Complex has been previously inferred based on ignimbrite stratigraphy and volcanic features (Lewis et al., 2025). The source vent of the Puripicar Ignimbrite is buried to the north of the Chaxas domes by overlying lavas of younger eruptive episodes associated with the Chaxas Complex and the modern volcanic arc (Figure 1). The volcano cluster above the Chaxas Volcanic Complex has a higher spatial vent density relative to the Andean arc (Supplementary File 2) due to the filtering effect of an inferred upper crustal plutonic complex remnant after ignimbrite volcanism (Baker, 1981, 1974; Lewis et al., 2025).

The Chaxas Volcanic Complex was built in two temporally distinct stages across multiple pulses of the APVC flare-up, as defined by the eruption ages previously described by Lewis et al. (2025) (Table 1). The Pre-Chaxas stage began with the 5.4 Ma Agua Perdida Rhyolite, followed by the ≥ 500 km^3 4.18 Ma Puripicar ignimbrite (PPI), and the 3.7 Ma Embaucador Rhyolite during the third pulse of the APVC flare-up. The Agua Perdida and Embaucador rhyolites are crystal poor (~10 % crystallinity) rhyolitic ignimbrites with a modal mineralogy comprised of plagioclase > quartz > biotite; the Embaucador contains sanidine. The Puripicar is a relatively well-studied "monotonous" crystal-rich dacite that has attracted numerous studies due to its extensive exposure and prominence as the plateau topping large ignimbrite along the Andean front (Brown et al., 2021; de Silva, 1989; Kern et al., 2016; Salisbury et al., 2011). As such it has been used as one of the archetypal large APVC crystal-rich dacitic ignimbrites that exemplify the flare-up.

The 3.5 – 1.2 Ma Chaxas Complex comprises a series of endogenous domes and deposits of block and ash flows, small pyroclastic density currents and pyroclastic fallouts at the southwestern margin of the APVC (Figure 1) that were produced dominantly during and after the final pulse of the APVC flare-up. Several thin pyroclastic fallout deposits are interspersed within the Chaxas Complex stratigraphy, including Pyroclastic Fallout I that lies unconformably on the Puripicar Ignimbrite at the base of the younger Chaxas Complex formation. The 3.7 km^3 Cerro Chaxas dome is the southernmost dome that was emplaced in the Chaxas dome complex at 1.9 Ma. The Cerro Chaxas dome is flanked to the west by a wedge of volcaniclastics that erupted from 2.8 – 1.8 Ma during phases of dome growth and collapse. The most prominent of these are referred to as the Youngest, Middle, and Oldest block and ash flows and are overlain by a small ignimbrite known as the Final del Agua Rhyolite.

Methodology

Zircon U-Pb Ages

All U-Pb zircon crystallization ages presented here were previously published by Lewis et al. (2025). Complete description of the analytical methodology is given in the supplementary material. Cathodoluminescence-images were taken at the Linus Pauling Institute at Oregon State University (OSU) prior to Laser Ablation – Inductively Coupled Plasma – Mass Spectrometer analyses using a ThermoFisher Scientific iCAP RQ quadrupole ICP-MS (LA-Q-ICP-MS) or a Nu Plasma 3D multicollector ICP-MS (LA-MC-ICP-MS) coupled to an Applied Spectra RESOlution-SE. At least one core and one rim analysis were analyzed when possible (i.e., when space and time provided), and some grains with complex CL-textures were measured on three spots. Prior to analysis in this study, it was necessary to remove U-Pb crystallization ages with large analytical uncertainties (> 15%), resulting in the removal of 137 LA-Q-ICP-MS analyses. All ages are included in Supplementary File 1. More than half of the remaining analyses were collected by LA-MC-ICP-MS. Instrumental parameters, U-Pb data, and standard reproducibility are tabulated in the supplementary materials. All uncertainties include analytical and systematic uncertainties that are propagated according to Horstwood et al. (2016) and are reported at the 2s level. In the results below, we report the range of U-Pb ages and define the difference between the oldest and youngest zircon as Δt.

Zircon Trace Elements and Ti-in-Zircon Temperatures

Trace element concentrations in zircon were determined using the same LA-Q-ICP-MS instrumentation used for U-Pb geochronology. CL-images were used to select spots in the same

growth zones that were selected for U-Pb geochronology when possible (i.e., not the same spot). Reference materials were analyzed in blocks every 20 analyses. All data were reduced using LaserTRAM-DB (Lubbers et al., 2025) with ^{29}Si as an internal standard and an assumed 32.8 wt % SiO_2. GSE-1G was used as a calibration reference material. All unknowns and a full list of analytes are reported in supplementary file 1.

Ti-in-zircon temperatures were calculated according to Ferry and Watson (2007). Quartz phenocrysts are present in the lithologies of all silicic rocks discussed here and so SiO_2 activity is assumed to be unity. TiO_2 activity is assumed to take on the nominal value of 0.6. This value is the intermediate value of ilmenite saturated silicic magmas (~ 0.5) and Ti-magnetite saturated silicic magmas (~ 0.7), both of which are present in the studied rocks and it can thus be reasonably assumed that the TiO_2 activity was buffered to ~ 0.6. We recognize that TiO_2 activity is known to vary in silicic magmas and that temperature estimates here could be compromised (e.g. Fonseca Teixeira et al., 2023). However, when propagating in uncertainties from the regression of Ferry and Watson (2007) as well as the uncertainty on ^{49}Ti measurements, changing the TiO_2 activity by ± 0.3 causes no difference in estimated crystallization temperatures and thus estimated temperatures here are viewed as accurate.

Results

Zircon U-Pb Crystallization Ages and CL-Textures

Pre-Chaxas Zircons

CL-textures and responses in Pre-Chaxas zircons are complex (Figure 3). Many grains show one or more truncations with oscillatory overgrowths. No consistent zoning pattern is present across grains with similar crystallization ages.

Crystallization ages gathered from zircon in the Agua Perdida Rhyolite are restricted to the second pulse of the APVC flare-up from 5.4 ± 0.4 Ma to 6.8 ± 0.5 Ma (Δt: 1.4 myr). These ages are overdispersed (MSWD = 3.6; n = 23). Puripicar Ignimbrite U-Pb crystallization ages are particularly overdispersed (MSWD = 9.7; n=67) with ages ranging from 8.7 ± 0.5 Ma to 4.6 ± 0.5 Ma. Zircon from the Puripicar define the largest Δt in all eruptive units presented here at 4.1 myr. This range extends from the first major pulse of the APVC flare-up at ca. 8.5 Ma to the second at ca. 4 Ma (Salisbury et al., 2011). Embaucador Rhyolite zircon crystallization ages have a range from 7.3 ± 0.8 Ma to 3.7 ± 0.3 Ma (Δt : 3.6 myr). These crystallization ages are also overdispersed (MSWD = 14.4; n = 62) and have a similar age range to the zircon crystallization ages in the Puripicar Ignimbrite.

Chaxas Complex Zircons

CL-textures and responses in Chaxas Complex zircons generally show oscillatory zoning and are typically gray to bright, particularly in block and ash flows. Generally, grains show CL-gray or CL-dark cores with progressively brighter overgrowths towards the rim (Figure 3).

Chaxas Complex U-Pb crystallization ages have significantly smaller ∆t values than the Pre-Chaxas eruptions when removing the outlier crystallization ages. Chaxas Complex eruptions carry zircons with discrete subpopulations of crystallization ages as well as individual crystallization ages that are outside of uncertainty from the primary age spectra (Figure 2). The oldest two eruptions of the Chaxas Complex have the most dispersed U-Pb crystallization ages. Zircon from the Oldest Block and Ash flow have crystallization ages ranging from 2.7 ± 0.5 Ma to 5.0 ± 0.5 Ma (∆t: 2.3 myr). Pyroclastic Fallout I zircon have a somewhat smaller range of ages from 3.5 ± 0.5 Ma to 5.2 ± 1.0 Ma (∆t : 1.7 myr). These crystallization ages overlap entirely with those in the Embaucador Rhyolite and Puripicar Ignimbrite (Figure 2). U-Pb ages collected by LA-Q-ICP-MS from the Oldest Block and Ash flow and Pyroclastic Fallout I are overdispersed despite large relative uncertainties (Figure 2).

Dome clasts as well as juvenile blocks from the block and ash flows have the narrowest distributions of U-Pb ages amongst eruptive units at the Chaxas Volcanic Complex. Zircon U-Pb ages from the Middle Block and Ash flow have a range of 2.3 ± 0.2 Ma to 2.6 ± 0.2 Ma. There is a single age outside of this range at 4.7 ± 0.3 Ma. Excluding this age results in an evenly dispersed set of U-Pb crystallization ages (MSWD = 0.7; n = 41) across a ∆t of only 300 kyr. U-Pb zircon ages from the Youngest Block and Ash flow are overdispersed (MSWD = 6.9, n=72) with a range of 1.8 ± 0.3 Ma to 4.2 ± 0.4 Ma (∆t: 2.4 myr). Cerro Chaxas U-Pb zircon ages have a small range of 1.9 ± 0.1 Ma to 2.8 ± 0.4 Ma (∆t: 900 kyr), with the exception of a single age that overlaps with Pre-Chaxas U-Pb ages at 6.3 ± 0.4 Ma.

The Final del Agua Rhyolite has an overdispersed set of U-Pb crystallization ages (MSWD = 37.1; n = 10) ranging from 1.1 ± 0.3 Ma to 4.1 ± 1.2 Ma (∆t: 3.0 myr) that are distributed across three distinct subpopulations. Within each of these subpopulations, zircon U-Pb crystallization ages are evenly dispersed.

Trace Elements

Pre-Chaxas Zircons

Trace element concentrations from Pre-Chaxas zircons display a relatively large range and can form distinct groups. Zircon from the Puripicar Ignimbrite show the greatest trace

element variation for a given set of zircons in an eruption. Zr/Hf in Puripicar zircons define two groups: high Zr/Hf zircons (Zr/Hf 48.8 – 55.3) and low Zr/Hf zircons (Zr/Hf: 36.4 – 43.9). Zr/Hf in zircons is positively correlated with Ti-in-zircon crystallization temperatures. High Zr/Hf correspond to a temperature range of 731 °C to 847 °C whereas low Zr/Hf zircons record low temperatures of 665 °C to 757 °C with little covariation. Th/U values negatively covary with the slope of HREE patterns, represented by Yb/Dy (Figure 5). Puripicar zircons have a broad range in the Eu anomaly (0.6 – 0.1), and the largest range of U concentrations of all eruptions (98 – 1063 µg/g). Zircons with the lowest U concentrations record the highest Ti-in-zircon temperatures.

Similar to those in the Puripicar, Embaucador zircons are split into two groups of low Zr/Hf (48.4 – 56.2) and high Zr/Hf (44 – 47). Zr/Hf in these zircons do not change predictably with Ti-in-zircon temperatures, similar to the low Zr/Hf zircons in the Puripicar. High Zr/Hf zircons in the Embaucador Rhyolite have somewhat elevated Th/U values. Th/U values of the Embaucador zircons have a subtle, negative correlation with Yb/Dy values.

Zr/Hf values of the Agua Perdida Rhyolite span a range similar to those seen in the other Pre-Chaxas eruptions. Similar to the Embaucador Rhyolite, Zr/Hf values of zircons in the Agua Perdida (45.5 – 50.6) also have little co-variation with Ti-in-zircon temperatures (737°C – 898°C). Only the zircons that record the lowest Ti-in-zircon temperatures (701°C – 721°C) have distinctly lower Zr/Hf values. Th/U values have a distinct, negative correlation between Th/U and Zr/Hf values. U concentrations of the Agua Perdida zircons span nearly the range of those seen in the Puripicar Ignimbrite.

Chaxas Complex Zircons

Chaxas Complex eruptions also carry zircons of diverse trace element concentrations, although the variation is more subtle. Dome lithologies in particular carry zircons that form a single dominant group within each eruption, with only subtle excursions towards more extreme values. This contrasts the Pre-Chaxas zircons that form discrete groups and large continuous arrays across their range of trace element concentrations (Figure 4, Figure 5).

Zircons from the Youngest Block and Ash flow have a limited range in U concentrations (187 – 527 µg/g), with few analyses falling outside of this range. Ti-in-zircon crystallization temperatures are dominantly grouped from 680°C – 748°C, though several analyses have temperatures from 776°C – 923°C. Zr/Hf values are generally tightly distributed from 39 – 45, though four analyses have Zr/Hf values up to 49 (Figure 4). Th/U values negatively covary with Yb/Dy values. Middle Block and Ash flow zircons show the most restricted range of trace

element data from all eruptive units. U concentrations of these zircons vary only from 189 – 413 µg/g across Ti-in-zircon crystallization temperatures of 719°C – 827°C. Zr/Hf (44 – 49) values also span a limited range relative to zircons in other eruptions. Zircon from Cerro Chaxas form two groups in trace elements, but it is important to note that the differences between the groups are substantially smaller than those observed in the Pre-Chaxas eruptions. A low U group (236 – 348 µg/g) and a high U group (594 – 642 µg/g) are present across Ti-in-zircon temperatures that range from 689°C – 776°C (Figure 4). One analysis has a higher temperature of 858°C, and another analysis has a high U concentration of 886 µg/g with a modest Ti-in-zircon crystallization temperature of 731 °C. Zr/Hf ratios of the Cerro Chaxas zircons that show two groups in U concentration are collapsed into a single group in Zr/Hf space with a fairly restricted range that is similar to that observed in the Middle and Youngest block and ash flows (Figure 4).

A few zircons from the Oldest Block and Ash flow were analyzed for trace element concentrations. Data that were gathered indicate a broad range of trace element concentrations that are similar to those in the Pre-Chaxas eruptions. Pyroclastic Fallout I zircons also have a broad range in trace element concentrations. Zr/Hf values range from 38.4 – 48.8 at relatively low Ti-in-zircon crystallization temperatures (682°C – 766°C). These zircons also have the steepest negative correlation between Yb/Dy and Th/U, and a distinct positive correlation between Zr/Hf and Th/U (Figure 5).

Discussion

Resolving Episodes of Crystallization and Cannibalization From Overdispersed U-Pb Datasets

Assessing the Value of the Mixed LA-Q-ICP-MS and LA-MC-ICP-MS U-Pb Datasets for Resolving U-Pb Subpopulations

All samples here show overdispersion according to the MSWD and its acceptable envelope (Wendt and Carl, 1991) prior to excluding outliers or identifying subpopulations, indicating that the range in U-Pb crystallization ages is not accounted for by the uncertainties. The MSWD has, however, come into scrutiny as large or even modest analytical uncertainties may result in MSWD values that have negligible differences from the value of their acceptable upper envelope based on observed and synthetically formulated zircon distributions that represent *a single cooling event* (Keller et al., 2018). Moreover, even when the MSWD does indicate overdispersion despite large uncertainties, the true duration of crystallization as well as the true underlying (certainly non-normal) distribution of apparent U-Pb ages *for a single cooling event* is probably lost to the uncertainties regardless (Klein and Eddy, 2023). Observed

distributions ultimately become increasingly normally distributed as analytical uncertainty increases. As a result of these issues, the statistic ∆t/s introduced by Keller et al. (2018) has been gaining popularity. Here, ∆t represents the range of crystallization ages (the convention used here) and s represents the average analytical uncertainty. The statistic ∆t/s is clearly interpretable and is not subject to confusion around what values indicate under-, even-, or overdispersion (note that overdispersion from the MSWD is a function of n, though many publications assume 1.0 as representing overdispersion). However, a critical weakness of the ∆t/s statistic is its lack of an envelope. Nathwani et al. (2025) performed an overview of high-precision datasets and characterized the relationship between U-Pb age distributions and ∆t/s. With ∆t/s values > 10, a systematic variation in the shapes of distributions and the types of rocks in which zircons are found (plutonic vs volcanic) is clear and geologically relevant, as volcanic rocks should naturally have truncated distributions and plutonic rocks should tend to show long lower tails due to slow cooling rates through the solidus. However, including datasets that have a ∆t/s of 5 – 10 results in substantially more normally distributed U-Pb datasets, which is consistent with modeling predictions that U-Pb ages with analytical uncertainties too large to be valuable will tend to show normal distributions (Klein and Eddy, 2023). Despite the lack of definitive statistical basis on what defines a dataset as overdispersed, ∆t/s are therefore reported in Figure 2. Almost all U-Pb datasets here have ∆t/s values much larger than 10 (Figure 2). Those datasets that do not are interpreted to represent much shorter durations of crystallization, as discussed in more detail below. As a result, the overdispersed U-Pb datasets reported here are interpreted to represent overdispersed datasets that represent either prolonged durations of crystallization or *multiple cooling events*.

The U-Pb dataset gathered here was first filtered for excessively large uncertainties, rendering a dataset that is mostly comprised of U-Pb ages determined by LA-MC-ICP-MS. This method typically has an order of magnitude better uncertainty than LA-Q-ICP-MS in the datasets presented here. For those samples where both LA-Q-ICP-MS and LA-MC-ICP-MS data are present, the observed ranges in U-Pb crystallization ages are recorded by both methodologies (Supplementary File 2). Furthermore, the crystallization ages from eruptions with large ∆t/s are indeed overdispersed according to the MSWD. On the other hand, the Middle Block and Ash flow has evenly dispersed, entirely overlapping U-Pb ages collected by LA-Q-ICP-MS and LA-MC-ICP-MS. U-Pb datasets presented in this manuscript (post-filtering) are therefore interpreted to represent accurate ∆t and show representative overdispersion, however hindered by poor precision. It is likely that more data collected by LA-MC-ICP-MS could provide sufficient *n* and precision to make more direct statistical inferences but at present this is

impossible given the uncertainties. First-order observation indicates that there is clearly unresolved structure within the U-Pb crystallization ages in each eruptive unit, although the analytical uncertainties are not sufficient to resolve any reliable multimodality.

Resolution of the Youngest Zircon Populations and Calculation of Δt_Y

Directly estimating a Δt to infer crystallization durations results in unreasonable estimates of upper crustal magmatic durations (Figure 6). Refinement of this variable requires resolution of the youngest zircon population and recalculation crystallization duration based on this autocrystic population. This value is reported here as Δt_Y. We therefore attempt to resolve the youngest population of U-Pb crystallization ages by utilizing the iterative MSWD approach, where U-Pb ages are iteratively added to the youngest set of ages until the upper envelope is exceeded (Stelten et al., 2015). Assuming that analytical artifacts, Pb-loss, mixing of age domains, and other potential issues with U-Pb ages have been accounted for or can be reasonably assumed to not dominate the U-Pb age distributions, U-Pb zircon ages can broadly represent 1) autocrystic ages representing crystallization of zircon (or intra-grain domains) within the youngest suprasolidus melt batch(es) that carried erupted material to the surface, 2) antecrystic ages or domains that represent crystallization from earlier magma batches which have been recycled into the youngest melt batch(es) that was either zircon saturated or had insufficient time for complete zircon resorption, 3) inherited zircons from a partial melting source prior to extraction of melt to the upper crust, or 4) xenocrystic zircons derived from host rocks that have relatively clear differences in crystallization age compared to the other populations (Miller et al., 2007). Here, those zircon ages that belong to the youngest population resolved by the iterative MSWD approach are interpreted to be autocrysts. All others are interpreted as antecrysts or xenocrysts. Pre-Chaxas units, particularly the Puripicar ignimbrite, carry a wide range of xenocrystic ages that indicate pervasive assimilation of local Andean crust, consistent with interpretations of Zr/Hf above. Further discussion of the significance of these zircon grains is presented elsewhere (Lewis et al., 2026).

After identifying the populations of autocrystic U-Pb zircon ages, Δt_Y was calculated from two methodologies. The first is simply the difference between the oldest and youngest U-Pb crystallization ages that provides a direct estimation for Δt_Y based simply on the data. The second calculation of Δt_Y was calculated according to the parameterization of Klein and Eddy (2023), which appropriately assumes a minimum duration if the MSWD of the crystallization ages is larger than the upper acceptable envelope value and a maximum duration if it is below.

The iterative MSWD method will always result in a maximum duration given that the iterations are ceased when the upper envelope of the MSWD will be exceeded.

Resulting Δt_Y values (Table 1) are all substantially lower and more reasonable than the unrealistic Δt values that range from > 1 to 4.1 myr (Figure 6), consistent with the fact that the longest recorded period of melt residence is approximately one myr; and this is an extreme residence time even amongst large caldera systems (c.f., Kaiser et al., 2017b; Wolff and Ramos, 2003). Below, all Δt_Y values discussed are those calculated by the parameterization of Klein and Eddy (2025) given that this method is descriptive in its assignment of maximum durations for the autocrystic subpopulations. The only exception to this is the Cerro Chaxas U-Pb crystallization ages, which has a young U-Pb crystallization age outside of uncertainty from the others.

Pre-Chaxas Magmatic Evolution – Development of the Super-Sized Puripicar Magma Reservoir

Prolonged Construction of the Composite Pre-Chaxas Magmatic System

Protracted zircon age spectra are particularly useful for deciphering the construction and evolving architecture within large silicic systems (Cisneros de León et al., 2021). Prolonged Δt of Pre-Chaxas zircons in particular attest to a long accumulation history that led to the eventual accumulation of at least 500 km^3 of eruptible magma prior to eruption of the Puripicar Ignimbrite, and certainly much more based on typical ratios of intrusive volumes to erupted volumes ("plutonic : volcanic ratios") of 6:1 to 10:1 for silicic magmatic systems (Crisp, 1984; White et al., 2006), and up to 32:1 – 70:1 for APVC magmatic systems constructed during the flare-up (Perkins et al., 2016; Tierney et al., 2016). Numerous crystallization events of zircon recorded by complex texture-age-trace element chemistry relationships (Figure 3) are interpreted to represent periods of episodic magmatic injection followed by cooling.

Early APVC magmatism at the Chaxas Volcanic Complex is documented by U-Pb crystallization ages spanning as far back as c.a. 9 Ma in the Puripicar Ignimbrite, suggesting that intrusive events occurred through the first and second major pulses of the APVC flare-up (Kern et al., 2016). Yet eruption from the Chaxas Volcanic Complex magmatic system did not occur until the second flare-up pulse with the eruption of the Agua Perdida Rhyolite at 5.44 Ma, followed more than one myrs later by the 4.18 Ma Puripicar supereruption and the 3.73 Ma Embaucador Rhyolite during the third pulse of the regional APVC flare-up (Table 1). Early, infrequent intrusions into magmatic systems that saw peak magmatic activity millions of years later across the APVC have been previously attributed to peripheral intrusive activity relative to

the loci of APVC volcanic activity (Kern et al. 2016). The initial constructive phases of the Chaxas Volcanic Complex magmatic system during the first-two pulses of the regional flare-up recorded by zircon U-Pb crystallization ages are interpreted to reflect this peripheral magmatic activity. Long-term construction of magmatic systems by episodic intrusion spanning millions of years has also been documented in exposed crustal sections with transient high flux marking the prolific periods of magma accumulation, crustal growth, and volcanism in these systems (Coleman et al., 2004; Eddy et al., 2022; Karakas et al., 2019; Klein et al., 2021; Samperton et al., 2015).

Evidence for composite construction in the Pre-Chaxas magmatic system is also seen in modeling results of U-Pb ages and trace element abundances in zircon. Final stages of magma accumulation for the Pre-Chaxas eruptions occurred over maximum durations of 420 to 600 thousand years, which is much shorter than the total Δt of millions of years (Figure 6). Residence times on the scale of hundreds of thousands of years are, however, long within the context of estimations for volcanic systems globally (Friedrichs et al., 2021; Pamukçu et al., 2025; Weber et al., 2023) but are consistent with the accumulation of large volumes of near- to suprasolidus silicic magma in upper crustal magmatic systems that can experience up to one million years of residence time (Barboni et al., 2016; Kaiser et al., 2017). Thermal models indicate that this could mean the reservoir experienced relatively high flux in order to incubate the system (de Silva and Gregg, 2014), which is consistent with higher assimilation rates in the Pre-Chaxas reservoir compared to the Chaxas Complex reservoir based on radiogenic isotope data (Lewis et al., 2026). Age constraints from a variety of magmatic systems also require that voluminous eruptions evacuated from reservoirs that stored large volumes of near-solidus material require transient increase in flux prior to eruption (Angeles-De La Torre et al., 2023; Rivera et al., 2016; Szymanowski et al., 2019) However, relatively low, constant flux rates may also produce prolonged residence times (Curry et al., 2021). This clearly introduces some ambiguity into the implications of the zircon crystallization ages and durations for the Pre-Chaxas eruptions.

Pre-Chaxas autocrysts and antecrysts have similar wide variation in trace element abundances (Figure 4), providing evidence for a composite volcanic system. Such consistent diversity seems to require relatively consistent influx of fresh magma and consequent thermal sustainment of a thermochemically diverse reservoir that fractionates between intrusive events. While a relatively logical line of explanation, trace element diversity is apparently entirely ambiguous when used to infer variation in magmatic input and thermochemical states of magmatic systems when accounting for age-trace element relationships. High trace element

diversity has been observed at the San Juan cluster which may have been constructed by relatively low, persistent flux followed by fresh magmatic input prior to eruption (Curry et al., 2021). Contrarily, transient high-flux in the Tocomar system in the APVC and the Tierra Blanca eruptive series of the Ilopongo caldera (Bardelli et al., 2026; Cisneros de León et al., 2021) produce higher trace element variation with increasing flux and eruptive volume. All of these interpretations contrast the Toba Caldera that shows a decrease in the range of trace element concentrations within zircon closer to eruption (Liu et al., 2021); which apparently requires constant flux with no increases prior to eruption. The differences in trace element systematics and zircon crystallization ages between systems such as Toba and the Chaxas Volcanic Complex can be reconciled by the proposal that there is no general model regarding flux and magmatic architectures appropriate for all large silicic reservoirs (Wilson et al., 2021), and each system should be viewed in its own context and modeling framework.

Collectively, prolonged zircon age spectra from the Pre-Chaxas eruptions record a long-lived, episodically recharged magmatic system that gradually accumulated large silicic volumes prior to peak activity. Early intrusions during the first two APVC flare-up pulses reflect peripheral magmatism and incremental construction of the Chaxas reservoir over nearly five myrs prior to catastrophic eruption. Lengthy Δt_Y values, complex zircon chemistries, and radiogenic isotopic signatures all indicate sustained crustal assimilation but cannot uniquely constrain the relative flux rate of the Pre-Chaxas magmatic system. Rather, features such as these are likely unique to the thermochemical state of the Pre-Chaxas magmatic system as they are in other magmatic systems.

Crustal Assimilation Recorded in Zircon Zr/Hf Ratios

Decreasing Zr/Hf values in zircon are typically thought to represent chemical differentiation of zircon saturated melt by co-crystallization of zircon, allanite, xenotime, or garnet, whereas co-saturated titanite and rutile would act to increase Zr/Hf due to their relative partition coefficients (Bea et al., 2006; Claiborne et al., 2006). Key natural datasets exhibiting this systematic decrease are observed in the Bergell intrusion and the Spirit Mountain batholith that record extensive zircon crystallization (Claiborne et al., 2006; Samperton et al., 2015). However, a group of zircons hosted in the rhyolitic Embaucador Rhyolite, Agua Perdida Rhyolite, and Puripicar Ignimbrite have the highest Zr/Hf values of all those measured in this study (Figure 5). Lack of clear trends between other geochemical proxies for fractionation and high Zr/Hf zircon rules out late saturation of zircon followed by extensive crystallization as an explanation for this observation. Calculated Zr saturation temperatures (Boehnke et al., 2013;

Harrison and Watson, 1983) of Puripicar Ignimbrite and Embaucador Rhyolite glasses are also unremarkably similar (Supplementary File 1), indicating zircon was probably continuously saturated during dacitic to rhyolitic melt production. These lines of evidence indicate that decreases in Zr/Hf ratios may not strictly reflect melt differentiation by crystallization of zircon or other Zr enriched phases. Comparison of Zr and Hf concentrations between whole rock (Zr/Hf: 29.8) and quenched anatectic melt (Zr/Hf: 41 - 47) of crustal xenoliths show that anatexis in some lithologies of the Andean crust will increase the Zr/Hf ratio of contaminated melt (McLeod et al., 2012).

High Zr/Hf ratios of zircons in evolved melts of the Chaxas Volcanic Complex magmatic system may result from melting of fertile upper crustal lithologies. Zircon is well-known to be one of the first phases resorbed during anatexis (Miller et al., 2007) resulting in enriched Zr/Hf values of anatectic melt. Allanite stability also connotes it would quickly become unstable during melting (Engi, 2017). Moreover, rutile and especially titanite are well-known reactants of melting reactions (Zack and Kooijman, 2017), which would enhance preferential liberation of Zr over Hf into resident magma during assimilation. Whatever the exact melting sequence, the enriched Zr/Hf ratios of partially melted crustal xenoliths from the Andes relative to the refractory material (McLeod et al., 2012) supports the inferences of trace element partitioning. To evaluate the feasibility of this model to explain the occurrence of high Zr/Hf ratios in evolved magmas at the Chaxas Volcanic Complex, trace element modeling via fractional crystallization with linear varying partition coefficients (Greenland, 1970) along with fractional crystallization and assimilation (FCA) models (Cribb and Barton, 1996) were performed. These latter models differ from a classic assimilation and fractional crystallization model (i.e., DePaolo, 1981), as they account for the common observation that crystallization and assimilation do not operate at the same rate (e.g., Angeles-De La Torre et al. 2023). Model results indicate that zircon trace element concentrations can generally be explained by fractional crystallization of silicic melt (Figure 5). High Zr/Hf zircons, however, are best explained by the FCA model. Zircons in evolved Pre-Chaxas magmas show that assimilation of crustal material must be included when interpreting trace element patterns in zircon with respect to Zr/Hf when there is a decoupling of Zr/Hf from other trace element proxies for fractionation, as high Zr/Hf zircon in rhyolites may signal an assimilation signature. These data are consistent with the high assimilation rates inferred for the large magmatic systems constructed during high flux in the APVC (de Silva et al., 2006; Grocke et al., 2017). An alternative explanation is that Zr and other trace element concentrations in silicic magmas may also be the result of cumulate melting. In this scenario, successive intrusions re-introduce and preferentially enrich trace elements that are compatible

to the resident mineralogy of a cumulate (Wolff et al., 2024). While this cannot be strictly ruled out, the assimilation signature interpreted here is preferred due to the observed Zr/Hf differences between crustal xenoliths and magmatic hosts within the Central Andes (McLeod et al., 2012).

In summary, elevated zircon Zr/Hf ratios in evolved Pre-Chaxas magmas reflect assimilation of fertile upper crustal lithologies rather than simple fractional crystallization. Modeling shows that fractional crystallization alone cannot reproduce the observed enrichment, whereas fractional crystallization–assimilation (FCA) models successfully account for high Zr/Hf values. These ratios likely record zircon resorption and liberation of Zr during crustal melting reactions also involving titanite and rutile. The decoupling of Zr/Hf from other differentiation proxies thus marks assimilation as a key process in the Chaxas magmatic system, consistent with isotopic and zircon xenocryst evidence for extensive crustal interaction during the Pre-Chaxas stage of the Chaxas Volcanic Complex (Lewis et al., 2026).

The Chaxas Complex –Distributed Upper Crustal Magmatism of Limited Persistence

Eruptions of the Chaxas Complex are substantially smaller in volume and restricted to the southern end of the Chaxas Volcanic Complex compared to the Pre-Chaxas (Figure 1), suggesting an overall decrease in the scale of the magmatic system. Many of these eruptions occurred in the transition between the third pulse of the APVC flare-up at c.a. 4 Ma and the fourth (waning) pulse of the flare-up at c.a. 2 ± 1 Ma. The focus of APVC magmatism had also shifted away from the Chaxas Volcanic Complex by 2 Ma (Kern et al., 2016), likely resulting in a decrease of magmatic influx into the Chaxas Volcanic Complex that could incubate large eruptions. Even a simple calculation of intrusive volumes estimated by extrusive volumes using global estimates of intrusive to extrusive ratios of 6:1 to 10:1 (Crisp, 1984; White et al., 2006) would result in two orders of magnitude difference in the volume of eruptible magma, as Chaxas Complex eruptions have volumes on the order of 1-5 km^3 contributing to an aggregate volume of ~10 km^3, whereas the Puripicar ignimbrite has an estimated volume of ca. 500 km^3 (de Silva, 1989; Lewis et al., 2025). However, it cannot be strictly ruled out that this ratio was constant between different eruptive phases given that small volume effusive volcanism in the APVC has also been linked to exceptional plutonic to volcanic ratios of 70:1 and relatively high magmatic flux (Tierney et al., 2016). One key observed difference between zircon distributions found in other dome complexes of the APVC constructed by high-flux (Tierney et al., 2016) and the

Chaxas Complex is Δt. Domes studied by Tierney et al. (2016) show fairly continuous zircon U-Pb age spectra while the zircon U-Pb age spectra of Chaxas Complex dome products have lower Δt's. While many of the U-Pb ages gathered here suffer from poor precision, most of the ages left after rejection (see methodology) from Middle Block and Ash flow as well as Cerro Chaxas are strictly much higher precision U-Pb ages collected by MC-ICP-MS (Figure 2), underscoring the observed differences.

Estimated maximum crystallization durations of the Chaxas Complex eruptions provide some evidence for magmatic input into the system during later stages of Chaxas Volcanic Complex lifecycle, though with some important limitations. Generally Δt_Y is similar between Chaxas Complex and Pre-Chaxas zircon U-Pb ages, but only when including those eruptions for which U-Pb crystallization ages were only gathered by LA-Q-ICP-MS. Excluding those eruptions (Final del Agua, Pyroclastic Fallout I, and Oldest Block and Ash flow), all other Chaxas Complex eruptions have zircon U-Pb distributions with Δt_Y ranging from essentially instantaneous to 400 kyr; or systematically shorter than those in Pre-Chaxas eruptions. These eruptions also carry clear antecrystic zircon populations even when considering the large uncertainties that characterize some of the data, indicating periods of substantial cooling and relatively impersistent magmatic influx that would otherwise create continuous U-Pb age distributions. These observations could be interpreted to represent that cannibalization of progenitor intrusions decreased systematically during the Chaxas Complex phase of magmatism. When considering the comparison to low volume effusive eruptions produced during high-flux in the APVC (Tierney et al., 2016), this would be consistent with observations that cannibalization is more efficient during punctuated periods of high flux (Rivera et al., 2016) should there be substantiative evidence that the flux-regime diminished between the Pre-Chaxas and Chaxas Complex stages.

Zircon trace element concentrations and textures observed in Chaxas Complex eruptions may provide some evidence for a decrease of ephemeral magma batches late in its history as trace element concentrations of these eruptions are more restricted within each individual unit. Specifically, U concentrations of the Middle Block and Ash flow are restricted to 200 – 400 µg/g and Ti-in-zircon crystallization temperatures vary within ~ 50 °C. The majority of zircon in the Youngest Block and Ash flow have low crystallization temperatures from 680 – 740 °C, and low U concentrations of ~ 180 – 550 µg/g (Figure 4). Similarly, Cerro Chaxas zircons show an extremely limited range in U concentrations of ~ 600 – 700 µg/g. These relative restrictions in trace element concentrations are also apparent in Zr/Hf, indicative of lower assimilation rates and a more restricted crystallization history. Only Pyroclastic Fallout I shows

extremely low Zr/Hf ratios, interpreted to represent more extensive fractionation of this relatively small volume eruption compared to the crystal-rich dacitic dome eruptions (Figure 5). Excursions of trace element concentrations and crystallization temperatures away from primary clusters of data are present but rare for Chaxas Complex eruptions (Figure 4, Figure 5). These excursions are in fact significant for the interpretation of the existence of small, ephemeral melt batches. Bimodality caused by infrequent recharge events during a relatively short lifecycle within a distributed magmatic system, or, initial crystallization following emplacement into the upper crust may be the cause of these trace element excursions. Crystallization temperatures of autocrystic Chaxas Complex zircons in particular indicate that the smaller, ephemeral melt batches did not efficiently buffer temperature perturbations (e.g., Black and Andrews, 2020). This is further supported by the antecrysts which have a more limited range in crystallization temperatures and much higher U concentrations, suggestive of near solidus crystallization (Troch et al., 2017). Indeed, such an interpretation of shorter melt residence and more ephemeral melt batches prior to Chaxas Complex eruptions compared to Pre-Chaxas eruptions complement zircon records which show tightly distributed age spectra are induced by sporadic recharge events during waning flux (Friedrichs et al., 2021). However, the data are relatively limited and we note that the wide range in crystallization temperatures that could be used to infer small volume magma batches during the Chaxas Complex stage is no different than those that could be used to interpret extensive compositional variation within a much larger magmatic reservoir for the Pre-Chaxas stage.

Zircon petrochronologic data of the eruptions of the Chaxas Complex may record waning magmatic flux and the transition from a large, integrated reservoir to small, short-lived magma batches. Shorter Δt_Y values support this but are hampered by poor precision that affects the estimation of crystallization durations. Trace-element variability may indicate diminished enthalpy budgets, weaker assimilation, and less efficient cannibalization of older intrusions although such inferences are weak within the context of current knowledge of zircon trace element systematics, as outlined above for the Pre-Chaxas stage. Besides inferring a constant plutonic:volcanic ratio, only the observation of systematic differences in the structure of U-Pb ages (Figure 2) and potentially inferring lower heat flux due to lower assimilation inferred from Zr/Hf and isotopic ratios (Lewis et al., 2026) could be used to infer the possibility that the flux regime changed between the Pre-Chaxas and Chaxas Complex stages. We therefore turn to thermal modeling to test the possibility of a change in flux regime more rigorously.

Varying Thermal Flux Controlling the Architecturally Evolving Magmatic System

Thermal Model Set-up and Motivation

Zircon U-Pb crystallization ages and variation trace element concentrations as well as constraints of magma flux that occurred during the pulsating APVC flare-up suggests a potential change in flux between the Pre-Chaxas stage and the Chaxas Complex stage. However, this inference is non-diagnostic based on the multi-entendre of reasonable interpretations of zircon systematics described above. Here we test the assertion that variation of magmatic flux in the Chaxas Volcanic Complex controls magmatic evolution and volcanic architecture, using thermal modeling techniques coupled with zircon crystallization ages (Angeles-De La Torre et al., 2023; Curry et al., 2021; Friedrichs et al., 2021; Liu et al., 2021; Tierney et al., 2016; Weber et al., 2020). Many of these studies quantify flux leading up to single eruptions or within a single flux regime (sometimes limited by secular equilibrium timescales), despite the characteristic lifecycle of caldera forming volcanic systems that frequently exhibit a slow but steady accumulation of magma, followed by high flux prior to the climactic phase, then finally distributed small volume upper crustal magmatism (Best et al., 2016; Black and Andrews, 2020; Folkes et al., 2011; Lipman, 1984; Szymanowski et al., 2019). The combined volcanic and zircon petrochronologic record at the Chaxas Volcanic Complex provides a unique opportunity to test if such inferences adequately explain variation in eruptive characteristics and complementary plutonic assemblage during ignimbrite flare-up magmatism.

Magmatic fluxes during the Pre-Chaxas and Chaxas Complex stage are estimated here by performing thermal models using the MagmaThermoKinematics open source program (Kaus et al., 2025), within which synthetic zircon distributions are formed by tracking temperatures to estimate the temperature dependent saturation of zircon (i.e., Caricchi et al., 2014; Schmitt et al., 2023). Model setups generally follow the so-called UCLA-HD approach which has been applied over decades (Angeles-De La Torre et al., 2023; Friedrichs et al., 2021; Schmitt et al., 2023b; Tierney et al., 2016). In this model approach, an elliptical intrusion with a sill like geometry (i.e., aspect ratio > 1) is assumed and recharge events are applied by injecting an ellipsoid into the center of the intrusion domain. In order to remain objective in our approach to testing if a flux differential exists between the Pre-Chaxas and Chaxas Complex stages, all magmatic injections were identical in temperature, size (3000m wide x 400m thick), and depth of intrusion. Constraints on the recharge temperature were set from estimations of APVC andesites (~1000 °C) that are small in volume but ubiquitous throughout the APVC (Burns and de Silva, 2023). Depth of intrusion was set to 8 km within an 80 km wide by 20 km deep domain, consistent with barometric estimates from the Puripicar ignimbrite (Lewis et al., 2026) and constraints of magmatic systems fed by the APMB batholith (Ward et al., 2014; Pritchard et al.,

2018; Pritchard and Gregg, 2016). Density and heat capacity for crustal host rocks were held constant at 2600 kg m^{-3} and 1050 J kg^{-1} K^{-1}, respectively. Thermal conductivity was temperature dependent (Whittington et al., 2009) and latent heat was set to 2.67 x 10^5 J kg^{-1}, although this held little consequence on synthetic zircon age distributions compared to other variables. For the Pre-Chaxas stage modeled using Puripicar U-Pb zircon ages, the bottom boundary condition assumes constant heat flux of 50 mW m^{-2}, or a third of the flux of the modern APMB (Pritchard et al., 2018), to approximate the typical flux while the APMB batholith was still being established. The bottom boundary condition during the Chaxas Complex stage, modeled by U-Pb zircon ages from the Middle Block and Ash flow, was set to higher 100 mW m^{-2}. The initial geothermal gradient showed the most significant control on melt fractions, average magmatic temperatures, and the resulting synthetic zircon age distributions. Even small variations of ca. 5°C greatly affect the feasibility of a given recharge history. Prior estimates of the geotherm resulting from flare-up magmatism of the Andes estimated a geotherm of 50°C km^{-1} based on a fully established APMB (de Silva and Gosnold, 2007). Given this and the location of the Chaxas Volcanic Complex at the edge of the APMB, where thermal perturbation exhibited by advection of magma from the APMB has less influence on peripheral magmatic systems (González-Maurel et al., 2019; Grunder et al., 2006; Lewis et al., 2022), an initial geothermal gradient of 30 °C km^{-1} was used for the Pre-Chaxas stage. A higher value of 35 °C km^{-1} was used for the Chaxas Complex stage. Tracers that track the time-temperature history were inserted with each dike for subsequent processing of synthetic zircon distributions using previously described methodology (Weber et al., 2020). Zircon saturation was assumed to occur at 900 °C, consistent with initial crystallization in an andesitic magma, and crystallization was assumed to stop at the granite solidus (690 °C). The temperatures sampled range from 840 – 690 °C for Puripicar (Pre-Chaxas) models and 830 – 720 °C for Middle Block and Ash flow (Chaxas Complex) models, consistent with autocryst crystallization temperatures (Figure 4). Due to computational constraints, model duration for the Puripicar Ignimbrite was set to 1.5 myr. Model duration for the magmatic history leading up to the Middle Block and Ash flow was set to 400 kyr. Below, all fluxes are reported in both traditional units (km^3 yr^{-1}) and intrusion area normalized units (km^3 yr^{-1} km^{-2}) in order to allow easy cross-comparison to magmatic reservoirs with different footprints that cool at different rates for a given input volume (Sliwinski et al., 2019).

Constraints on Pre-Chaxas Reservoir Flux from Zircon U-Pb Ages

Models of constant flux for the Pre-Chaxas stage were attempted to be benchmarked and broadly constrained by constant flux models ranging from 1.0 x 10^{-5} km^3 yr^{-1} to 6.5 x 10^{-2} km^3 yr^{-1}. Not one of these models was able to reproduce the observed Puripicar U-Pb crystallization ages due to the predominance of young zircon that result in a strongly concave cumulative distribution function (CDF) – an apparently common issue when modeling synthetic zircon distributions (Angeles-De La Torre et al., 2023). In addition, models with high flux rates of 1 x 10^{-3} km^3 yr^{-1} to 8 x 10^{-5} km^3 yr^{-1} followed by cooling (i.e., cessation of all recharge) for anywhere from 250 kyr to 1100 kyr also failed to reproduce the observed distribution either due to the domain being entirely subsolidus or having a large zircon fraction occurring during only part of the model time, again resulting in a concave CDF that could not reproduce the slightly convex distribution of Puripicar U-Pb ages used for the modeling approach (Figure 7). Failure of these approaches indicate that a pulsed intrusive history is the most likely scenario for the Pre-Chaxas reservoir, as inferred for the pre-eruptive magmatic history of large eruptions (e.g., Rivera et al., 2016; Szymanowski et al., 2019)

Initial flux in the pulsed intrusive models were found to require a high pulse in order to induce prolific crystallization early in the history. Lack of such an initial pulse results in the concavity described above for the same reasons. This is also geologically reasonable given that the model start occurs at approximately 6 Ma during the second major pulse of the APVC (Kern et al., 2016) after rescaling the synthetic zircon ages (Figure 7). Relatively low flux near the end of the model also produces a much steeper synthetic CDF slope that contrasts strongly with the gentle slope in the CDF of the observed U-Pb ages, due to much of the intrusive volume being within the observed Ti-in-zircon crystallization temperature window of PPI zircons (Figure 4) used to resample the tracers. Modeling transient, steep slopes in the CDF that may indicate periods of cooling also requires approximately an order of magnitude difference in flux – area normalized or otherwise. However, interpreting these features may also be misleading due to the large uncertainties and thus multiple intrusive histories produce reasonable synthetic zircon age distributions.

Two flux histories were found that produce synthetic zircon distributions which agree with the observed U-Pb distribution for the 1.5 myr crystallization history prior to the eruption of the PPI. The first is a near constant flux model with intrusions that occur once every 15 kyr and a pulse of intrusions at the beginning and end of the modeled time domain. In this scenario, the flux of the Pre-Chaxas magmatic system is estimated to be 1.2 x 10^{-3} km^3 yr^{-1} (1.7 x 10^{-4} km^3 yr^{-1} km^{-2}) with a total intrusive volume of 1776 km^3. Another plausible intrusive history has an additional period of relatively high flux from 900 – 950 kyr of the total 1500 kyr history, which

was modeled to ensure continuous magma residence for 600 kyr estimated by zircon crystallization durations (Figure 6). For this scenario the flux is a similar to the near constant flux model, with an estimate of 1.7 x 10^{-3} km^3 yr^{-1} (2.3 x 10^{-4} km^3 yr^{-1} km^{-2}) and pulses of flux up to 6.28 x 10^{-3} km^3 yr^{-1}. The total intrusive volume across the same time domain is notably higher at 2481 km^3. Based on the constraints provided by the U-Pb crystallization duration, it is likely that this latter model is more accurate although we cannot rule out the possibility that the "lower" flux scenario is possible based on the uncertainties of the U-Pb ages. Assuming similar flux rates across the entire crystallization history recorded by the PPI these two models produce a total intrusive volume estimate of 4854 – 6781 km^3. Intrusive to extrusive volumes in the upper crustal pre-eruptive reservoir based on these estimates is well within estimates for silicic volcanism at 9.7 – 13.6.

Constraints on the Younger Stage, Chaxas Complex Flux from Zircon U-Pb Ages

Models using a constant flux rate were tested for the Chaxas Complex stage, with fluxes ranging from 1.05 x 10^{-6} km^3 yr^{-1} to 1.05 x 10^{-3} km^3 yr^{-1}. None of these models were able to reproduce the observed slightly concave U-Pb zircon age spectra observed from the Middle Block and Ash Flow (Figure 7). Similarly, models that produced constant flux of similar magnitudes followed by cooling periods failed to reproduce the observed zircon U-Pb age spectra. The observed U-Pb distribution was ultimately constrained by bracketing the observed distribution between two models of near constant flux interrupted by short periods of high magmatic input or cooling. In the first scenario, the model begins with a period of relatively high flux rates characterized by intrusions occurring every 1 kyr for 50 kyr. This is followed by a prolonged period of intrusions occurring every 20 kyr for another 320 kyr. Another pulse occurs for the final 20 kyr of the 400 kyr model time domain, with intrusions again occurring every 1 kyr. This results in an average flux of 4.0 x 10^{-4} km^3 yr^{-1} (5.6 x 10^{-5} km^3 yr^{-1} km^{-2}) with a total volume of 158 km^3. This ultimately results in a flux that is too high for most of the model domain, but we attempt to bracket this with a different modeling approach that allows a period of cooling followed by recharge at the end of the model (i.e., just before eruption). In this case, intrusions occur every 1 kyr for only 20 kyr followed up again by intrusions occurring every 15 kyr, but here flux ceases after an additional 300 kyr. A final intrusive period then occurs 390 kyr into the model time domain, with intrusions occurring every 1 kyr. For this modeled scenario the total intrusive volume is much smaller than the first (91 km^3) and the average flux is slightly smaller at 2.2 x 10^{-4} km^3 yr^{-1} (3.2 x 10^{-5} km^3 yr^{-1} km^{-2}). Due to the evenly dispersed U-Pb dataset of the antecrystic zircons in this eruption, we prefer the former higher flux of these two models as this

intrusion history results in a persistent magma intrusion that is likely more representative of the U-Pb ages. However, we cannot rule out the possibility that the magma reservoir was not persistent for this entire period due to the relatively large uncertainties and modeled results which suggest this scenario could be possible.

According to the models that bracket the Middle Block and Ash flow zircons, flux during the Chaxas Complex stage diminished significantly compared to the Pre-Chaxas stage (Figure 7), with an estimated range of 2.2 x 10^{-4} km^3 yr^{-1} to 4.0 x 10^{-4} km^3 yr^{-1} (2.3 x 10^{-5} km^3 yr^{-1} km^{-2} to 3.2 x 10^{-5} km^3 yr^{-1} km^{-2}). This flux estimate is a maximum, because the modeled synthetic zircon distribution used to derive a flux estimate for the Middle Block and Ash flow (Figure 7) is compared to a set of zircon ages with even dispersion, which could represent a single intrusive event. Overall, significantly lower thermal fluxes are recorded in the zircon spectra of the Chaxas Complex eruptions compared with those estimated for the Pre-Chaxas stage represented by Puripicar Ignimbrite crystallization ages.

Implications of Variable Flux Rates at the Chaxas Volcanic Complex

Flux estimates ranging from 1.45 x 10^{-3} km^3 yr^{-1} up to 6.28 x 10^{-3} km^3 yr^{-1} made by multiple models for the Pre-Chaxas stage are on the order of magnitude estimated for the formation of large upper crustal reservoirs that birth voluminous eruptions (Gelman et al., 2013) and slightly higher than the late Pleistocene lava domes in the APVC that were extracted from a thermally contiguous upper crustal zone that sustained several small widely separated melt zones (Tierney et al., 2016). The flux and the thermal history of the Chaxas Complex as modelled by the Middle Block and Ash flow is nearly an order of magnitude lower than the Pre-Chaxas stage of the magmatic system. The estimate of 1.6 x 10^{-4} km^3 yr^{-1} to 4.0 x 10^{-4} km^3 yr^{-1} is typical of steady state (long term secular background) fluxes estimated for volcanic arcs, including the Andes (Bertin et al., 2023; Jicha and Jagoutz, 2015). This is consistent with the Chaxas Complex being constructed under the post-flare-up, waning flux regime of the APVC.

Compared to flux estimates for the region that rely on assumptions of volcanic to plutonic ratios (Bertin et al., 2023; de Silva and Gosnold, 2007), the flux estimates made here are either the same or approximately one order of magnitude lower. Higher flux estimates of 1.2 x 10^{-2} –6 x 10^{-2} km^3 yr^{-1} (de Silva and Gosnold, 2007) are attributed to integrating the volumes over short periods of pulses on the order of a few hundred thousand years. More recent estimations found the intrusive flux for the region to average 4.8 x 10^{-4} km^3 yr^{-1} for a 23 km section of arc like the Chaxas Volcanic Complex, and up to 1.2 x 10^{-2} km^3 yr^{-1} for the highest instantaneous flux estimates (Bertin et al., 2023), which overlaps with the range of fluxes

estimated for the Chaxas Volcanic Complex. Differences for the region can ultimately be attributed to assumptions about the time domain over which the volumes are integrated, and ultimately all of these assumptions still put the flux estimates for the Pre-Chaxas reservoir well above the 20 km^3 / one km of arc / one million year flux estimate that is considered the baseline for magmatic flare-ups (Jicha and Jagoutz, 2015).

One of the primary motivations for modeling flux between representative eruptions of the Pre-Chaxas and Chaxas Complex stages is to highlight the rate of change of magmatic flux within a large silicic system throughout its lifecycle. The Pre-Chaxas stage ended at c.a. 4.0 Ma, with eruption of the Puripicar Ignimbrite occurring at 4.18 Ma and the Embaucador Rhyolite approximately four hundred thousand years later at 3.73 Ma. No large eruptions or stratigraphically continuous rhyolitic tuffs were emplaced following the Pre-Chaxas stage. Only Pyroclastic Fallout I, a volumetrically insignificant eruption (Lewis et al., 2025) erupted at 3.54 Ma after the Embaucador Rhyolite and before the first signs of dome activity with emplacement of the Oldest Block and Ash flow at 2.75 Ma. Moreover, zircon U-Pb crystallization ages in Pyroclastic Fallout I could be interpreted as representing the same crystallization event as the most recent that occurred prior to eruption of the Embaucador Rhyolite (Figure 2). As such, it is interpreted that the average magmatic flux into the Chaxas Volcanic Complex changed systematically between eruption of the Embaucador Rhyolite and emplacement of the Oldest Block and Ash flow at the latest, and probably by the time Pyroclastic Fallout I erupted. Assuming the modeling results are representative for the contrasting high and low flux stages of magmatism within the Chaxas Volcanic Complex, this indicates that magmatic flux shifted by an order of magnitude within a period of c.a. 200 kyr. Relatively rapid cessation of high magmatic flux into the system may result from efficient refocusing of magmatic activity from the APMB (Kern et al., 2016).

Altogether, thermal modeling and zircon petrochronology reveal that magmatic flux at the Chaxas Volcanic Complex declined by roughly an order of magnitude between the Pre-Chaxas and Chaxas Complex stages. High-flux conditions with pulses up to 6.28 x 10^{-3} km^3 yr^{-1} and a long term average of 1.45 x 10^{-3} km^3 yr^{-1} (2 x 10^{-4} km^3 yr^{-1} km^{-2}) sustained long-lived magma accumulation and supereruption potential during the Pre-Chaxas stage, whereas the Chaxas Complex stage operated at background steady state arc-flux levels (≤ ~ 4.0 x 10^{-4} km^3 yr^{-1}), producing small, short-lived magma batches. Modeling further indicates that this transition occurred within ~ 200 kyr—an abrupt thermal and magmatic reorganization linked to regional refocusing of flux away from Chaxas. These results demonstrate that large silicic systems can experience rapid, order-of-magnitude changes in flux that controls their thermal longevity,

architecture, and eruptive output with the ultimate tangible result being the achievement of magmatic repose within geologically short time intervals.

Reconstructing the Architecture of the Remnant Composite Plutonic System Beneath the Chaxas Volcanic Complex

One of the primary interests for estimating intrusive volumes and magmatic flux rates is to provide insight into the link between volumetric production of volcanoes and their subcrustal plutonic complexes. Estimating how these intrusive complexes are assembled and whether or not their assemblage is characterized by relatively persistent flux that creates a more homogenous system (Liu et al., 2021), or incremental assembly from pulsating magmatic flux that results in compositionally, thermally, and structurally complex systems (Krueger and Yoshinobu, 2018; Matzel et al., 2006) provides insights into the rates of upper crustal magmatic assemblage and if large volumes of magma can potentially be stored in the upper crust. Flux and volume estimates from the thermal models and zircon crystallization ages as well as trace element concentrations are therefore compared here to well-constrained plutonic and volcanic systems in the literature to evaluate and analyze the significance of the results in this study.

Flux estimates for Pre-Chaxas eruptions are lower than the extensive Southern Rocky Mountain Volcanic Field (SRMVF) that has an estimated flux of 5 x 10^{-2} km^3 yr^{-1} (Lipman and Bachmann, 2015) and contains numerous caldera complexes underpinned by batholiths with volumes on the order of 10^3 km^3. The flux and volume estimate from the Puripicar Ignimbrite is expectedly smaller than more voluminous flare-ups such as the SRMVF (Best et al., 2016). Rather, the Pre-Chaxas flux estimates (~ 1.45 x 10^{-3} km^3 yr^{-1}; 2 x 10^{-4} km^3 yr^{-1} km^{-2}) and volume (~ 5800 km^3) are directly comparable to the 3.5 x 10^{-3} km^3 yr^{-1} flux and 1200 – 9000 km^3 volume estimated for the long-lived and voluminous Mt. Stuart pluton (Lipman and Bachmann, 2015; Matzel et al., 2006). Interestingly, the best-fit intrusive history for the Pre-Chaxas magmatic history that accounts for the variable slope in the empirical cumulative distribution of the observed U-Pb crystallization ages of the Puripicar Ignimbrite (Figure 7) is characterized by pulses of high flux separated by lower flux conditions, similar to that observed at the Mt. Stuart pluton. Sharp geochronological discontinuities across otherwise compositionally homogenous silicic domains within Mt. Stuart also attest to its incremental, upper crustal history. As an intrusive proxy to the volcanic Chaxas Volcanic Complex, the similar magmatic history and characteristics observed at the Mt. Stuart batholith indicates that the large and long-lived volcanic system that produced the Puripicar Ignimbrite is now underpinned by a similar composite, silicic plutonic complex. As regional flux waned, however, the intrusive volume into

the upper crust drastically diminished to a maximum of 100's of km^3 at a single period and likely less based on this estimate being an upper bound for the Middle Block and Ash flow (Figure 7). Using the 158 km^3 estimated intrusion history across the 400 kyr time domain modeled for the Middle Block and Ash flow crystallization history, no more than 790 km^3 of magma was emplaced during the entire Chaxas Complex stage. As supported by the trace element concentrations and crystallization ages of the Chaxas Complex eruptions, the resident melt during the latter stages of the Chaxas Volcanic Complex was likely short and emplaced into a voluminous silicic mush that had largely solidified following catastrophic eruption and peak magmatic activity (Figure 8). These results imply that the dominant volume of the plutonic system beneath the Chaxas Volcanic Complex was emplaced during the Pre-Chaxas stage, and indeed that large volumes of magma must have been stored in the upper crust prior to eruption of the Puripicar Ignimbrite. Results here also corroborate prior work which has shown that assuming a plutonic:volcanic ratio of ~ 6:1 – 10:1 for low volcanic flux regimes may cause a severe underestimation of the intrusive volume of magma (Tierney et al., 2016). Whereas the high flux Pre-Chaxas stage prior to eruption of the Puripicar Ignimbrite exhibits a plutonic:volcanic ratio of 9.7 – 13.6, the Chaxas Complex stage of substantially lower volcanic flux has a plutonic:volcanic ratio of approximately 79:1 based on the estimated 10 km^3 of erupted dome lithologies. This emphasizes that even relatively low volcanic flux can be accompanied by volumetrically significant intrusive activity (Mills and Coleman, 2013; Tappa et al., 2011; Tierney et al., 2016).

In summary, thermal modeling of zircon petrochronology indicates that the Chaxas Volcanic Complex is underpinned by a composite plutonic system assembled predominantly during the high-flux Pre-Chaxas stage. Intrusive volumes of ~ 5800 km^3 and fluxes as high as 6.28×10^{-3} km^3 yr^{-1} parallel those of incrementally constructed batholiths like Mt. Stuart, suggesting episodic, pulsed assembly of a large silicic reservoir. During the waning Chaxas Complex stage, intrusive volumes fell to ≤ 1500 km^3, yielding an extreme plutonic : volcanic ratio (~ 150:1) despite low eruptive output. These results imply that most upper-crustal magma accumulation occurred rapidly during peak flux, with later injections limited to minor replenishment of a cooling silicic mush—preserving a fossilized plutonic architecture beneath the Chaxas Volcanic Complex.

At a broader scale, both variance and invariance of magmatic flux have been recorded in volcanic systems. Volcanic systems that have experienced multiple large eruptions or caldera collapse events have been interpreted to experience multiple pulses of upper crustal magmatism, as constrained by short durations of crystallization (Gaynor et al., 2023; Rivera et

al., 2016) or sustained moderate flux, as constrained by zircon crystallization ages and thermal modeling (Curry et al., 2021; Liu et al., 2021). For systems like the Chaxas Volcanic Complex with only one catastrophic eruption produced during a stage of notably high magmatic (or volcanic) flux, it is likely that the dominant magmatic volume is produced during a relatively short time interval relative to the entire lifecycle.

Conclusions

The volcanic record of the Chaxas Volcanic Complex is inferred to record a transition from large-volume, integrated magmatism during the Pre-Chaxas stage (5.44 – 3.73 Ma) to lower-volume, spatially distributed magmatism during the Chaxas Complex phase (3.54 – 1.24 Ma). This evolution parallels the inferred thermal trajectory of the Altiplano-Puna Volcanic Complex (APVC) ignimbrite flare-up. Through the lens of zircon petrochronology this study has demonstrated how variations in magmatic flux governed the development and architecture of the Chaxas Volcanic Complex and its plutonic underpinnings. The analysis and interpretation of zircon petrochronologic data lead to the following conclusions:

1) Zircon petrochronology of the Chaxas Volcanic Complex reveals that its magmatic evolution was governed by cyclic variations in thermal and magmatic flux that drove a transition from prolonged upper-crustal magma assembly to distributed, waning magmatism.
2) The distinction between autocrystic and antecrystic zircon populations by the widely applied iterative MSWD approach defines melt-residence durations (Δt_Y) and reveals that older zircon and domains were recycled from remnant progenitor intrusions during successive recharge. Textural truncations, trace-element variability, and the presence of inherited and xenocrystic grains collectively indicate repeated rejuvenation and assimilation of crustal material.
3) Elevated zircon Zr/Hf ratios in Pre-Chaxas eruptions require fractional-crystallization–assimilation processes rather than simple differentiation, linking high Zr/Hf values to crustal melting reactions involving titanite and rutile during high-flux stages.
4) Thermal modeling and zircon petrochronology reveal that early Pre-Chaxas magmatism was characterized by long-lived, episodic intrusions emplaced at fluxes averaging ~ 1.45×10^{-3} $km^3\ yr^{-1}$ (2×10^{-4} $km^3\ yr^{-1}\ km^{-2}$). These conditions incubated a supereruption-scale magma body and extensive crustal assimilation leading to the Puripicar supereruption. Following the APVC flare-up peak, flux waned by an order of magnitude (≤ 4.0×10^{-4} $km^3\ yr^{-1}$; 5.6×10^{-5} $km^3\ yr^{-1}\ km^{-2}$), producing smaller, short-lived magma batches and more compositionally

uniform zircon populations. The transition occurred within ~ 200 kyr, marking rapid thermal and structural reorganization of the system.

5) Thermal and flux modeling, supported by zircon age distributions, suggest that the Chaxas system is underpinned by a composite plutonic complex assembled largely during the high-flux Pre-Chaxas stage (4854 - 6781 km^3). Younger Chaxas Complex intrusions (≤ 800 km^3) represent minor replenishment of a cooling silicic mush, yielding a high plutonic:volcanic ratio (~ 79:1). Collectively, these findings show that large silicic systems evolve through pulsed magmatic fluxes that control reservoir architecture, eruptibility, and plutonic construction.

Acknowledgements

CTL is indebted to the Geological Society of America, the Sharp family, the Mazamas mountaineering organization, and the Central Oregon Geoscience Society for their various funding initiatives that made this work possible. CTL is supported through a Graduate Research Assistantship where he works in the W.M. Keck Collaboratory at Oregon State University. This work was not possible without the encouragement and comradery of Chris Russo and Adam Kent. We are grateful for Christian Metzke of Alma Gaucho Expeditions, Matias Villaroel, and Alex Cisneros who helped us in the field. Logistical support and sample export from Chile was enabled by Felipe Aguilera (Universidad del Norte) and Benigno Godoy (Universidad de Chile). Axel Schmitt provided insightful comment on an earlier version of this manuscript. CTL acknowledges the critical contribution of Katherine Worms in ensuring the thermal models ran without interruption. Lorenzo Tavazzani and an anonymous reviewer provided thorough critiques that greatly strengthened this manuscript. Dr. Marco Fiorentini provided excellent editorial handling to see this manuscript published.

Table 1: Generalized Stratigraphy and U-Pb age durations of Chaxas Volcanic Complex

Formation	Unit	Eruption Age (Ma)	Eruption Type	Δt	Δt_Y
Chaxas Complex	Final del Agua Rhyolite	1.24 ± 0.05	PDC	3.02	≤ 0.17*
	Youngest B&A	1.83 ± 0.01	B&A	2.43	≤ 0.41
	Cerro Chaxas	1.86 ± 0.06	Dome	4.43	^
	Middle B&A	2.35 ± 0.01	B&A	2.47	≤ 0.32
	Oldest B&A	2.75 ± 0.19	B&A	2.25	≤ 9.4
	Pyroclastic Fallout I	3.54 ± 0.33	PF	1.65	≤1.0*
Pre-Chaxas	Embaucador Rhyolite	3.73 ± 0.02	PDC	3.52	≤ 0.43
	Puripicar Ignimbrite	4.18 ± 0.03	PDC	4.17	≤ 0.60
	Agua Perdida Rhyolite	5.44 ± 0.01	PDC	1.32	≤ 0.59

All eruption ages from Lewis et al. (2025), except the Puripicar Ignimbrite age from Brown et al. (2021). PDC: Pyroclastic Density Current. B&A: Block and Ash Flow. PF: Pyroclastic Fallout.

Δt: Range of crystallization ages (myr) defined by difference of oldest and youngest U-Pb crystallization ages

Δt_Y: Crystallization duration of autocrystic subpopulation (myr) determined by iterative MSWD method. Durations from Klein and Eddy (2025) unless specified.

*Duration is subject to large uncertainty as data are from LA-Q-ICP-MS only
^: Youngest U-Pb age is outside of uncertainty from the rest of the U-Pb ages within the sample

References

Angeles-De La Torre, C.A., Schmitt, A.K., Lovera, O.M., Gassert, H., Gerdes, A., Harvey, J.C., 2023. A common magma source for plutonic and volcanic rocks of The Geysers geothermal field, California: Volume and intrusive history derived from zircon. Chemical Geology 624, 121414. https://doi.org/10.1016/j.chemgeo.2023.121414

Baker, M.C.W., 1981. The nature and distribution of upper cenozoic ignimbrite centres in the Central Andes. Journal of Volcanology and Geothermal Research 11, 293–315. https://doi.org/10.1016/0377-0273(81)90028-7

Baker, M.C.W., 1974. Volcano spacing, fractures, and thickness of the lithosphere — A discussion. Earth and Planetary Science Letters 23, 161–162. https://doi.org/10.1016/0012-821X(74)90186-1

Barboni, M., Annen, C., Schoene, B., 2015. Evaluating the construction and evolution of upper crustal magma reservoirs with coupled U/Pb zircon geochronology and thermal modeling: A case study from the Mt. Capanne pluton (Elba, Italy). Earth and Planetary Science Letters 432, 436–448. https://doi.org/10.1016/j.epsl.2015.09.043

Barboni, M., Boehnke, P., Schmitt, A.K., Mark Harrison, T., Shane, P., Bouvier, A.S., Baumgartner, L., 2016. Warm storage for arc magmas. Proceedings of the National Academy of Sciences of the United States of America 113, 13959–13964. https://doi.org/10.1073/pnas.1616129113

Bardelli, L., Filipovich, R., Báez, W., Becchio, R., Arnosio, M., Schmitt, A.K., Danišík, M., Zhang, C., Monaco, L., Giaccio, B., De Astis, G., Viramonte, J., Giordano, G., 2026. Crystallinity variability in rhyolites: Insights from the Tocomar volcanic system (Puna Plateau, NW Argentina). Journal of Volcanology and Geothermal Research 473, 108581. https://doi.org/10.1016/j.jvolgeores.2026.108581

Bea, F., Montero, P., Ortega, M., 2006. A LA-ICP-MS EVALUATION OF Zr RESERVOIRS IN COMMON CRUSTAL ROCKS: IMPLICATIONS FOR Zr AND Hf GEOCHEMISTRY, AND ZIRCON-FORMING PROCESSES. The Canadian Mineralogist 44, 693–714. https://doi.org/10.2113/gscanmin.44.3.693

Bertin, D., De Silva, S.L., Lindsay, J.M., Cronin, S.J., Caffe, P.J., Connor, C.B., Grosse, P., Báez, W., Bustos, E., Constantinescu, R., 2023. Magmatic addition rates differentiate periods of steady-state versus flare-up magmatism in the Central Andean arc. Commun Earth Environ 4, 75. https://doi.org/10.1038/s43247-023-00744-2

Best, M.G., Christiansen, E.H., de Silva, S., Lipman, P.W., 2016. Slab-rollback ignimbrite flareups in the southern Great Basin and other Cenozoic American arcs: A distinct style of arc volcanism. Geosphere 12, 1097–1135. https://doi.org/10.1130/GES01285.1

Black, B.A., Andrews, B.J., 2020. Petrologic imaging of the architecture of magma reservoirs feeding caldera-forming eruptions. Earth and Planetary Science Letters 552, 116572. https://doi.org/10.1016/j.epsl.2020.116572

Boehnke, P., Watson, E.B., Trail, D., Harrison, T.M., Schmitt, A.K., 2013. Zircon saturation re-revisited. Chemical Geology 351, 324–334. https://doi.org/10.1016/j.chemgeo.2013.05.028

Brown, L., Singer, B.S., Barquero-Molina, M., 2021. Paleomagnetism and 40Ar/39Ar chronology of ignimbrites and lava flows, Central Volcanic Zone, Northern Chile. Journal of South American Earth Sciences 106, 103037. https://doi.org/10.1016/j.jsames.2020.103037

Burns, D.H., de Silva, S.L., 2023. Andesites and evolution of the continental crust: Perspectives from the Central Volcanic Zone of the Andes. Front. Earth Sci. 10, 961130. https://doi.org/10.3389/feart.2022.961130

Burns, D.H., de Silva, S.L., Tepley, F., Schmitt, A.K., Loewen, M.W., 2015. Recording the transition from flare-up to steady-state arc magmatism at the Purico-Chascon volcanic

complex, northern Chile. Earth and Planetary Science Letters 422, 75–86. https://doi.org/10.1016/j.epsl.2015.04.002
Caricchi, L., Simpson, G., Schaltegger, U., 2014. Zircons reveal magma fluxes in the Earth' s crust. Nature 511, 457–461. https://doi.org/10.1038/nature13532
Cisneros de León, A., Schmitt, A.K., Kutterolf, S., Schindlbeck- Belo, J.C., Hernández, W., Sims, K.W.W., Garrison, J., Kant, L.B., Weber, B., Wang, K. - L., Lee, H. - Y., Trumbull, R.B., 2021. Zircon and Melt Extraction From a Long- Lived and Vertically Extensive Magma System Underneath Ilopango Caldera (El Salvador). Geochem Geophys Geosyst 22. https://doi.org/10.1029/2020GC009507
Claiborne, L., Miller, C.F., Walker, B.A., Wooden, J.L., Mazdab, F.K., Bea, F., 2006. Tracking magmatic processes through Zr/Hf ratios in rocks and Hf and Ti zoning in zircons: An example from the Spirit Mountain batholith, Nevada. Mineral. mag. 70, 517–543. https://doi.org/10.1180/0026461067050348
Coleman, D.S., Gray, W., Glazner, A.F., 2004. Rethinking the emplacement and evolution of zoned plutons: Geochronologic evidence for incremental assembly of the Tuolumne Intrusive Suite, California. Geology 32, 433–436. https://doi.org/10.1130/G20220.1
Coney, P.J., Reynolds, S.J., 1977. Cordilleran Benioff zones. Nature 270, 403–406. https://doi.org/10.1038/270403a0
Cribb, J.W., Barton, M., 1996. Geochemical effects of decoupled fractional crystallization and crustal assimilation. Lithos 37, 293–307. https://doi.org/10.1016/0024-4937(95)00027-5
Crisp, J.A., 1984. Rates of magma emplacement and volcanic output. Journal of Volcanology and Geothermal Research 20, 177–211. https://doi.org/10.1016/0377-0273(84)90039-8
Curry, A., Gaynor, S.P., Davies, J.H.F.L., Ovtcharova, M., Simpson, G., Caricchi, L., 2021. Timescales and thermal evolution of large silicic magma reservoirs during an ignimbrite flare-up: perspectives from zircon. Contrib Mineral Petrol 176, 103. https://doi.org/10.1007/s00410-021-01862-w
de Silva, S., Kay, S.M., 2018. Turning up the heat: High-flux magmatism in the central andes. Elements 14, 245–250. https://doi.org/10.2138/gselements.14.4.245
de Silva, S., Self, S., 2022. Capturing the Extreme in Volcanology: The Case for the Term "Supervolcano." Front. Earth Sci. 10, 859237. https://doi.org/10.3389/feart.2022.859237
de Silva, S., Zandt, G., Trumbull, R., Viramonte, J.G., Salas, G., Jiménez, N., 2006. Large ignimbrite eruptions and volcano-tectonic depressions in the Central Andes: A thermomechanical perspective. Geological Society Special Publication 269, 47–63. https://doi.org/10.1144/GSL.SP.2006.269.01.04
de Silva, S.L., 1989. Geochronology and stratigraphy of the ignimbrites from the 21 ° 30' S to 23 ° 30' S portion of the Central Andes of Northern Chile.
de Silva, S.L., Gosnold, W.D., 2007. Episodic construction of batholiths: Insights from the spatiotemporal development of an ignimbrite flare-up. Journal of Volcanology and Geothermal Research 167, 320–335. https://doi.org/10.1016/j.jvolgeores.2007.07.015
de Silva, S.L., Riggs, N.R., Barth, A.P., 2015. Quickening the Pulse: Fractal Tempos in Continental Arc Magmatism. Elements 11, 113–118. https://doi.org/10.2113/gselements.11.2.113
DePaolo, D.J., 1981. Trace element and isotopc effects of combined wallrock assimilation and fractional crystallization. Earth and Planetary Science Letters 53, 189–202.
Eddy, M.P., Pamukçu, A., Schoene, B., Steiner-Leach, T., Bell, E.A., 2022. Constraints on the timescales and processes that led to high-SiO2 rhyolite production in the Searchlight pluton, Nevada, USA. Geosphere 18, 1000–1019. https://doi.org/10.1130/GES02439.1
Engi, M., 2017. Petrochronology Based on REE-Minerals: Monazite, Allanite, Xenotime, Apatite. Reviews in Mineralogy and Geochemistry 83, 365–418. https://doi.org/10.2138/rmg.2017.83.12

Farina, F., Weber, G., Hartung, E., Rubatto, D., Forni, F., Luisier, C., Caricchi, L., 2024. Magma flux variations triggering shallow-level emplacement of the Takidani pluton (Japan): Insights into the volcanic-plutonic connection. Earth and Planetary Science Letters 635, 118688. https://doi.org/10.1016/j.epsl.2024.118688

Ferry, J.M., Watson, E.B., 2007. New thermodynamic models and revised calibrations for the Ti-in-zircon and Zr-in-rutile thermometers. Contrib Mineral Petrol 154, 429–437. https://doi.org/10.1007/s00410-007-0201-0

Folkes, C.B., Wright, H.M., Cas, R.A.F., de Silva, S.L., Lesti, C., Viramonte, J.G., 2011. A re-appraisal of the stratigraphy and volcanology of the Cerro Galán volcanic system, NW Argentina. Bulletin of Volcanology 73, 1427–1454. https://doi.org/10.1007/s00445-011-0459-y

Fonseca Teixeira, L.M., Troch, J., Bachmann, O., 2023. The dynamic nature of *a* TiO2: Implications for Ti-based thermometers in magmatic systems. Geology. https://doi.org/10.1130/G51587.1

Friedrichs, B., Schmitt, A.K., Lovera, O.M., Atıcı, G., 2021. Zircon as a recorder of contrasting magma recharge and eruptive recurrence patterns. Earth and Planetary Science Letters 571, 117104. https://doi.org/10.1016/j.epsl.2021.117104

Gaynor, S.P., Smith, T.M., Schaltegger, U., 2023. Tracing magmatic genesis and evolution through single zircon crystals from successive supereruptions from the Socorro Caldera Complex, USA. Earth and Planetary Science Letters 616, 118236. https://doi.org/10.1016/j.epsl.2023.118236

Gelman, S.E., Gutiérrez, F.J., Bachmann, O., 2013. On the longevity of large upper crustal silicic magma reservoirs. Geology 41, 759–762. https://doi.org/10.1130/G34241.1

González-Maurel, O., le Roux, P., Godoy, B., Troll, V.R., Deegan, F.M., Menzies, A., 2019. The great escape: Petrogenesis of low-silica volcanism of Pliocene to Quaternary age associated with the Altiplano-Puna Volcanic Complex of northern Chile (21°10′-22°50′S). Lithos 346–347. https://doi.org/10.1016/j.lithos.2019.105162

Greenland, L.P., 1970. An equation for trace element distribution during magmatic crystallization. The American Mineralogist 55, 455–465.

Grocke, S.B., Andrews, B.J., de Silva, S.L., 2017. Experimental and petrological constraints on long-term magma dynamics and post-climactic eruptions at the Cerro Galán caldera system, NW Argentina. Journal of Volcanology and Geothermal Research 347, 296–311. https://doi.org/10.1016/j.jvolgeores.2017.09.021

Grunder, A.L., Klemetti, E.W., Feeley, T.C., McKee, C.M., 2006. Eleven million years of arc volcanism at the Aucanquilcha Volcanic Cluster, northern Chilean Andes: implications for the life span and emplacement of plutons. Transactions of the Royal Society of Edinburgh: Earth Sciences 97, 415–436. https://doi.org/10.1017/S0263593300001541

Harrison, T.M., Watson, E.B., 1983. Kinetics of zircon dissolution and zirconium diffusion in granitic melts of variable water content. Contr. Mineral. and Petrol. 84, 66–72. https://doi.org/10.1007/BF01132331

Hildreth, W., 1981. Gradients in silicic magma chambers: implications for lithospheric magmatism., Journal of Geophysical Research. https://doi.org/10.1029/JB086iB11p10153

Horstwood, M.S.A., Košler, J., Gehrels, G., Jackson, S.E., McLean, N.M., Paton, C., Pearson, N.J., Sircombe, K., Sylvester, P., Vermeesch, P., Bowring, J.F., Condon, D.J., Schoene, B., 2016. Community- Derived Standards for LA - ICP - MS U- (Th-)Pb Geochronology – Uncertainty Propagation, Age Interpretation and Data Reporting. Geostand Geoanal Res 40, 311–332. https://doi.org/10.1111/j.1751-908X.2016.00379.x

Jicha, B.R., Jagoutz, O., 2015. Magma Production Rates for Intraoceanic Arcs. Elements 11, 105–111. https://doi.org/10.2113/gselements.11.2.105

Kaiser, J.F., de Silva, S., Schmitt, A.K., Economos, R., Sunagua, M., 2017a. Million-year melt–presence in monotonous intermediate magma for a volcanic–plutonic assemblage in the Central Andes: Contrasting histories of crystal-rich and crystal-poor super-sized silicic magmas. Earth and Planetary Science Letters 457, 73–86. https://doi.org/10.1016/j.epsl.2016.09.048

Kaiser, J.F., de Silva, S., Schmitt, A.K., Economos, R., Sunagua, M., 2017b. Million-year melt–presence in monotonous intermediate magma for a volcanic–plutonic assemblage in the Central Andes: Contrasting histories of crystal-rich and crystal-poor super-sized silicic magmas. Earth and Planetary Science Letters 457, 73–86. https://doi.org/10.1016/j.epsl.2016.09.048

Karakas, O., Wotzlaw, J.-F., Guillong, M., Ulmer, P., Brack, P., Economos, R., Bergantz, G.W., Sinigoi, S., Bachmann, O., 2019. The pace of crustal-scale magma accretion and differentiation beneath silicic caldera volcanoes. Geology 47, 719–723. https://doi.org/10.1130/G46020.1

Kaus, B., Aellig, P., de Montserrat, A., 2025. MagmaThermoKinematics. https://doi.org/10.5281/ZENODO.15741541

Kay, S.M., Coira, B.L., Caffe, P.J., Chen, C.H., 2010. Regional chemical diversity, crustal and mantle sources and evolution of central Andean Puna plateau ignimbrites. Journal of Volcanology and Geothermal Research 198, 81–111. https://doi.org/10.1016/j.jvolgeores.2010.08.013

Keller, C.B., Schoene, B., Samperton, K.M., 2018. A stochastic sampling approach to zircon eruption age interpretation. Geochemical Perspective Letters LLNL-JRNL.

Kern, J.M., de Silva, S.L., Schmitt, A.K., Kaiser, J.F., Iriarte, A.R., Economos, R., 2016. Geochronological imaging of an episodically constructed subvolcanic batholith: U-Pb in zircon chronochemistry of the Altiplano-Puna Volcanic Complex of the Central Andes. Geosphere 12, 1054–1077. https://doi.org/10.1130/GES01258.1

Klein, B.Z., Eddy, M.P., 2023. What's in an age? Calculation and interpretation of ages and durations from U-Pb zircon geochronology of igneous rocks. Geological Society of America Bulletin. https://doi.org/10.1130/B36686.1

Klein, B.Z., Jagoutz, O., Ramezani, J., 2021. High-precision geochronology requires that ultrafast mantle-derived magmatic fluxes built the transcrustal Bear Valley Intrusive Suite, Sierra Nevada, California, USA. Geology 49, 106–110. https://doi.org/10.1130/G47952.1

Krueger, R.J., Yoshinobu, A.S., 2018. Structures in the Jackass Lakes pluton–host-rock system, central Sierra Nevada, California, and inferred mid-Cretaceous Farallon–North America plate kinematics. GSA Bulletin 130, 1940–1958. https://doi.org/10.1130/B31992.1

Lewis, C., de Silva, S., Cisneros De Leon, A., Alohali, A., 2026. Magmatic flux influences chemical heterogeneity of the Chaxas volcanic complex, N. Chile. Lithos 524–525, 108417. https://doi.org/10.1016/j.lithos.2026.108417

Lewis, C., de Silva, S., Cisneros De Leon, A., Burns, D., Villarroel, M., 2025. Effusive volcanic microcosm of a regional ignimbrite flare-up: Prolonged life cycle of the Chaxas Complex, northern Chile, and its influence on modern volcanic arc character. Geological Society of America Bulletin. https://doi.org/10.1130/B37909.1

Lewis, C.T., de Silva, S.L., Burns, D.H., 2022. Rhyolitic melt production in the midst of a continental arc flare-up—The heterogeneous Caspana ignimbrite of the Altiplano-Puna volcanic complex of the Central Andes. Geosphere 18, 1679–1709. https://doi.org/10.1130/GES02462.1

Lipman, P.W., 1984. The roots of ash flow calderas in western North America: Windows into the tops of granitic batholiths. J. Geophys. Res. 89, 8801. https://doi.org/10.1029/JB089iB10p08801

Lipman, P.W., Bachmann, O., 2015. Ignimbrites to batholiths: Integrating perspectives from geological, geophysical, and geochronological data. Geosphere 11, 705–743. https://doi.org/10.1130/GES01091.1

Lipman, P.W., Doe, B.R., Hedge, C.E., Steven, T.A., 1978. Petrologic evolution of the San Juan volcanic field, southwestern Colorado: Pb and Sr isotope evidence. Geol Soc America Bull 89, 59. https://doi.org/10.1130/0016-7606(1978)89%253C59:PEOTSJ%253E2.0.CO;2

Liu, P.-P., Caricchi, L., Chung, S.-L., Li, X.-H., Li, Q.-L., Zhou, M.-F., Lai, Y.-M., Ghani, A.A., Sihotang, T., Sheldrake, T.E., Simpson, G., 2021. Growth and thermal maturation of the Toba magma reservoir. Proc. Natl. Acad. Sci. U.S.A. 118, e2101695118. https://doi.org/10.1073/pnas.2101695118

Lubbers, J., Kent, A.J.R., Russo, C., 2025. lasertram: A Python library for time resolved analysis of laser ablation inductively coupled plasma mass spectrometry data. Applied Computing and Geosciences 100225. https://doi.org/10.1016/j.acags.2025.100225

Matzel, J.E.P., Bowring, S.A., Miller, R.B., 2006. Time scales of pluton construction at differing crustal levels: Examples from the Mount Stuart and Tenpeak intrusions, North Cascades, Washington. Geological Society of America Bulletin 118, 1412–1430. https://doi.org/10.1130/B25923.1

McLeod, C.L., Davidson, J.P., Nowell, G.M., de Silva, S.L., 2012. Disequilibrium melting during crustal anatexis and implications for modeling open magmatic systems. Geology 40, 435–438. https://doi.org/10.1130/G33000.1

Miller, J.S., Matzel, J.E.P., Miller, C.F., Burgess, S.D., Miller, R.B., 2007. Zircon growth and recycling during the assembly of large, composite arc plutons. Journal of Volcanology and Geothermal Research 167, 282–299. https://doi.org/10.1016/j.jvolgeores.2007.04.019

Mills, R.D., Coleman, D.S., 2013. Temporal and chemical connections between plutons and ignimbrites from the Mount Princeton magmatic center. Contrib Mineral Petrol 165, 961–980. https://doi.org/10.1007/s00410-012-0843-4

Nathwani, C., Szymanowski, D., Tavazzani, L., Markovic, S., Virmond, A.L., Chelle-Michou, C., 2025. Controls on zircon age distributions in volcanic, porphyry and plutonic rocks. Geochronology 7, 15–33. https://doi.org/10.5194/gchron-7-15-2025

Pamukçu, A.S., Hickernell, S.M., Eddy, M.P., Schoene, B., Steiner-Leach, T., 2025. Geology constrains the diffusivity of Ti in quartz and crystallization timescales of high-silica magmas in the Searchlight Magmatic System (NV, USA). Earth and Planetary Science Letters 666, 119437. https://doi.org/10.1016/j.epsl.2025.119437

Perkins, J.P., Ward, K.M., de Silva, S.L., Zandt, G., Beck, S.L., Finnegan, N.J., 2016. Surface uplift in the Central Andes driven by growth of the Altiplano Puna Magma Body. Nat Commun 7, 13185. https://doi.org/10.1038/ncomms13185

Pritchard, M.E., de Silva, S.L., Michelfelder, G., Zandt, G., McNutt, S.R., Gottsmann, J., West, M.E., Blundy, J., Christensen, D.H., Finnegan, N.J., Minaya, E., Sparks, R.S.J., Sunagua, M., Unsworth, M.J., Alvizuri, C., Comeau, M.J., del Potro, R., Díaz, D., Diez, M., Farrell, A., Henderson, S.T., Jay, J.A., Lopez, T., Legrand, D., Naranjo, J.A., McFarlin, H., Muir, D., Perkins, J.P., Spica, Z., Wilder, A., Ward, K.M., 2018. Synthesis: PLUTONS: Investigating the relationship between pluton growth and volcanism in the Central Andes. Geosphere 14, 954–982. https://doi.org/10.1130/GES01578.1

Pritchard, M.E., Gregg, P.M., 2016. Geophysical evidence for silicic crustal melt in the continents: Where, what kind, and how much? Elements 12, 121–127. https://doi.org/10.2113/gselements.12.2.121

Rivera, T.A., Schmitz, M.D., Jicha, B.R., Crowley, J.L., 2016. Zircon Petrochronology and 40 Ar/39Ar Sanidine Dates for the Mesa Falls Tuff: Crystal-scale Records of Magmatic

Evolution and the Short Lifespan of a Large Yellowstone Magma Chamber. J. Petrology 1677–1704. https://doi.org/10.1093/petrology/egw053

Salisbury, M.J., Jicha, B.R., de Silva, S.L., Singer, B.S., Jiménez, N.C., Ort, M.H., 2011. 40Ar/39Ar chronostratigraphy of Altiplano-Puna volcanic complex ignimbrites reveals the development of a major magmatic province. Bulletin of the Geological Society of America 123, 821–840. https://doi.org/10.1130/B30280.1

Samperton, K.M., Bell, E.A., Barboni, M., Keller, C.B., Schoene, B., 2017. Zircon age-temperature-compositional spectra in plutonic rocks. Geology 45, 983–986. https://doi.org/10.1130/G38645.1

Samperton, K.M., Schoene, B., Cottle, J.M., Brenhin Keller, C., Crowley, J.L., Schmitz, M.D., 2015. Magma emplacement, differentiation and cooling in the middle crust: Integrated zircon geochronological–geochemical constraints from the Bergell Intrusion, Central Alps. Chemical Geology 417, 322–340. https://doi.org/10.1016/j.chemgeo.2015.10.024

Schmitt, A.K., Sliwinski, J., Caricchi, L., Bachmann, O., Riel, N., Kaus, B.J.P., Cisneros De Léon, A., Cornet, J., Friedrichs, B., Lovera, O., Sheldrake, T., Weber, G., 2023a. Zircon age spectra to quantify magma evolution. Geosphere 19, 1006–1031. https://doi.org/10.1130/GES02563.1

Schmitt, A.K., Sliwinski, J., Caricchi, L., Bachmann, O., Riel, N., Kaus, B.J.P., Cisneros De Léon, A., Cornet, J., Friedrichs, B., Lovera, O., Sheldrake, T., Weber, G., 2023b. Zircon age spectra to quantify magma evolution. Geosphere 19, 1006–1031. https://doi.org/10.1130/GES02563.1

Schmitt, A.K., Vazquez, J.A., 2017. Secondary Ionization Mass Spectrometry Analysis in Petrochronology. Reviews in Mineralogy and Geochemistry 83, 199–230. https://doi.org/10.2138/rmg.2017.83.7

Sliwinski, J., Farsky, D., Lipman, P.W., Guillong, M., Bachmann, O., 2019. Rapid Magma Generation or Shared Magmatic Reservoir? Petrology and Geochronology of the Rat Creek and Nelson Mountain Tuffs, CO, USA. Front. Earth Sci. 7, 271. https://doi.org/10.3389/feart.2019.00271

Stelten, M.E., Cooper, K.M., Vazquez, J.A., Calvert, A.T., Glessner, J.J.G., 2015. Mechanisms and Timescales of Generating Eruptible Rhyolitic Magmas at Yellowstone Caldera from Zircon and Sanidine Geochronology and Geochemistry. J. Petrology 56, 1607–1642. https://doi.org/10.1093/petrology/egv047

Szymanowski, D., Ellis, B.S., Wotzlaw, J.-F., Bachmann, O., 2019. Maturation and rejuvenation of a silicic magma reservoir: High-resolution chronology of the Kneeling Nun Tuff. Earth and Planetary Science Letters 510, 103–115. https://doi.org/10.1016/j.epsl.2019.01.007

Tappa, M.J., Coleman, D.S., Mills, R.D., Samperton, K.M., 2011. The plutonic record of a silicic ignimbrite from the Latir volcanic field, New Mexico: PLUTON-IGNIMBRITE CONNECTIONS, QUESTA, NM. Geochem. Geophys. Geosyst. 12, n/a-n/a. https://doi.org/10.1029/2011GC003700

Tavazzani, L., Peres, S., Sinigoi, S., Demarchi, G., Economos, R.C., Quick, J.E., 2020. Timescales and mechanisms of crystal-mush rejuvenation and melt extraction recorded in Permian plutonic and volcanic rocks of the Sesia Magmatic System (southern Alps, Italy). Journal of Petrology 61. https://doi.org/10.1093/petrology/egaa049

Tavazzani, L., Wotzlaw, J.-F., Economos, R., Sinigoi, S., Demarchi, G., Szymanowski, D., Laurent, O., Bachmann, O., Chelle-Michou, C., 2023. High-precision zircon age spectra record the dynamics and evolution of large open-system silicic magma reservoirs. Earth and Planetary Science Letters 623, 118432. https://doi.org/10.1016/j.epsl.2023.118432

Tierney, C.R., Schmitt, A.K., Lovera, O.M., de Silva, S.L., 2016. Voluminous plutonism during volcanic quiescence revealed by thermochemical modeling of zircon. Geology 44, 683–686. https://doi.org/10.1130/G37968.1

Troch, J., Ellis, B.S., Mark, D.F., Bindeman, I.N., Kent, A.J.R., Guillong, M., Bachmann, O., 2017. Rhyolite generation prior to a yellowstone supereruption: Insights from the Island Park-Mount Jackson rhyolite series. Journal of Petrology 58, 29–52. https://doi.org/10.1093/petrology/egw071

Walker, B.A., Grunder, A.L., Wooden, J.L., 2010. Organization and thermal maturation of long-lived arc systems: Evidence from zircons at the Aucanquilcha volcanic cluster, northern Chile. Geology 38, 1007–1010. https://doi.org/10.1130/G31226.1

Ward, K.M., Zandt, G., Beck, S.L., Christensen, D.H., McFarlin, H., 2014. Seismic imaging of the magmatic underpinnings beneath the Altiplano-Puna volcanic complex from the joint inversion of surface wave dispersion and receiver functions. Earth and Planetary Science Letters 404, 43–53. https://doi.org/10.1016/j.epsl.2014.07.022

Weber, G., Blundy, J., Bevan, D., 2023. Mush Amalgamation, Short Residence, and Sparse Detectability of Eruptible Magma Before Andean Super- Eruptions. Geochem Geophys Geosyst 24, e2022GC010732. https://doi.org/10.1029/2022GC010732

Weber, G., Caricchi, L., Arce, J.L., Schmitt, A.K., 2020. Determining the current size and state of subvolcanic magma reservoirs. Nature Communications 11. https://doi.org/10.1038/s41467-020-19084-2

Wendt, I., Carl, C., 1991. The statistical distribution of the mean squared weighted deviation. Chemical Geology: Isotope Geoscience section 86, 275–285. https://doi.org/10.1016/0168-9622(91)90010-T

White, S.M., Crisp, J.A., Spera, F.J., 2006. Long-term volumetric eruption rates and magma budgets. Geochemistry, Geophysics, Geosystems 7. https://doi.org/10.1029/2005GC001002

Whittington, A.G., Hofmeister, A.M., Nabelek, P.I., 2009. Temperature-dependent thermal diffusivity of the Earth's crust and implications for magmatism. Nature 458, 319–321. https://doi.org/10.1038/nature07818

Wilson, C.J.N., Cooper, G.F., Chamberlain, K.J., Barker, S.J., Myers, M.L., Illsley-Kemp, F., Farrell, J., 2021. No single model for supersized eruptions and their magma bodies, Nature Reviews Earth and Environment. https://doi.org/10.1038/s43017-021-00191-7

Wolff, J.A., Ramos, F.C., 2003. Pb isotope variations among Bandelier Tuff feldspar: No evidence for a long-lived silicic magma chamber. Geology 31, 533–536. https://doi.org/10.1130/0091-7613(2003)031%253C0533:PIVABT%253E2.0.CO;2

Wolff, J.A., Ramos, F.C., Boro, J.R., Olin, P.H., Self, S., Winters, R.L., Kuentz, D.C., Dimond, C., Cook, G.W., Kyle, P.R., 2024. Compositional zoning of the Otowi Member of the Bandelier Tuff, Valles caldera, New Mexico, USA. Geosphere 20, 315–344. https://doi.org/10.1130/GES02618.1

Zack, T., Kooijman, E., 2017. Petrology and Geochronology of Rutile. Reviews in Mineralogy and Geochemistry 83, 443–467. https://doi.org/10.2138/rmg.2017.83.14

Declaration of interests

☒ The authors declare that they have no known competing financial interests or personal relationships that could have appeared to influence the work reported in this paper.

☐ The authors declare the following financial interests/personal relationships which may be considered as potential competing interests:

Figure Captions

Figure 1

Map of the Chaxas Volcanic Complex adapted from (Lewis et al., 2025) showing the extent of eruptive units. Black solid line shows Chilean-Bolivian border. The Puripicar Ignimbrite is volumetrically dominant with respect to all other eruptions from the Chaxas Volcanic Complex. Pre-Chaxas eruptions, including the Puripicar Ignimbrite, are stratigraphically beneath the Youngest Block and Ash Flow at the west side of the Chaxas Dome Complex. Dashed outlines show the inferred footprint of the underlying magmatic reservoirs during the two eruptive stages.

Figure 2

Diagram showing rank order U-Pb zircon ages from eruptions of the Chaxas Volcanic Complex. Eruption age of units increases towards the right. MSWD, range of crystallization ages (Δt), and the ratio of the range of crystallization ages and average analytical uncertainty (Δt/s) are shown above each of the datasets. MSWD* and Δt* indicates the values of these statistics after removing the clear antecrysts that are outside of the rest of the otherwise evenly dispersed population of U-Pb ages.

Figure 3

Representative cathodoluminescence (CL-) images from eruptive units of the two major stages of volcanic activity at the Chaxas Volcanic Complex. Zircon grains from the Pre-Chaxas stage are internally complex. These grains show multiple truncations and overgrowths likely representing repeated growth and dissolution. Zircon grains from the Chaxas Complex stage show less textural complexity. Zoning in these grains is generally oscillatory. Many grains have a similar bright CL-response near or at the rim.

Figure 4

A,B) Zircon Ti concentrations vs U concentrations and Zr/Hf. Dashed grey lines show Ti concentration at a given temperature (Ferry and Watson, 2007). A general increase in U concentration with decreasing temperature is present, although a wide variety of temperatures at low degrees of evolution imply high thermal gradients or recharge events. Zr/Hf also decreases with decreasing temperature, but it should be noted that zircon groups with higher Zr/Hf values do not correlate with decreasing Ti-in-zircon crystallization temperatures. Pre-Chaxas eruptions carry zircons that form distinct groups and/or relatively continuous arrays of data. Chaxas Complex zircons tend to be more tightly grouped.

C, D) Age constrained trace element data. Autocrystic zircon from the Chaxas Complex is less dispersed than autocrystic zircon from the Pre-Chaxas eruptions and have Zr/Hf values that correlate more readily with variations in temperature, consistent with the presence of small, relatively homogenous melt batches with a simple cooling history.

Figure 5

Zircon trace element analyses for each eruptive unit with modeled fractional crystallization (FC) and fractional crystallization and assimilation (FCA) trends. Solid and dashed lines show FC and FCA trends, respectively. Solid black numbers show percentage of melt remaining in the model. Black and purple models show modeled trends using the PPI and ER as starting compositions, respectively. A) Zr/Hf vs Th/U values. Note that decreasing Zr/Hf values are interpreted to indicate progressive melt evolution, but the evolved ER, APR, and PPI carry the highest Zr/Hf that are best explained by assimilation of high Zr/Hf melt. B) Eu/Eu* vs U concentrations. Models here bracket the data array, supporting that melt evolution formed progressively high U, low Eu/Eu zircons. C) Yb/Dy vs Th/U values. Two distinct trends defining a low and high Yb/Dy trend are interpreted from the dataset. Lower trend formed primarily by ER zircons is best explained by FC of rhyolitic melt. All other data fall between the models that describe melt evolution within the system.

Figure 6

Diagram showing estimated crystallization durations of autocrystic zircon subpopulations (referred to as Δt_Y in the text) determined from the iterative MSWD approach and total range of U-Pb crystallization ages (Δt). Maximum crystallization durations (following Klein and Eddy, (2025)) of these autocrystic subpopulations are within uncertainty of the rudimentary Δt_Y calculated as the difference between the oldest and youngest autocrystic zircons identified from mixture modeling. Crystallization durations are assigned a maximum due to their MSWD being below the threshold value for the acceptable MSWD. Durations of the entire series of U-Pb crystallization ages within each eruptive unit, which are clearly unreasonable estimates for residence times, are shown for comparison. Durations of crystallization estimated from autocrystic zircon populations (Δt_Y) are substantially shorter than the total range of crystallization ages and fall within reasonable residence times. Cerro Chaxas has a U-Pb crystallization age that falls outside of uncertainty from the rest of the data, interpreted to indicate a final crystallization event occurred during final ascent.

Figure 7

Diagrams showing cumulative probability of U-Pb zircon crystallization ages (black lines) with fitted synthetic zircon distributions produced from thermal models. Also shown are the thermal histories of the models as represented by the mean and standard deviation of the tracer temperatures throughout the model time. Observed range of Ti-in-zircon crystallization temperatures shown as light red fields. A) Empirical zircon U-Pb age CDF from the Middle Block and Ash Flow shown with the synthetic zircon distributions retrieved from the tracers within the thermal models. Note the flux estimate for the MBA is a maximum because the age data are underdispersed. B) Thermal histories from the tracers with the same symbology as in (A). The higher flux model has supra-solidus temperature throughout the entire history. Perturbations in temperature result from intrusions. Lower melt volumes are more sensitive to thermal perturbation, indicated as higher variability of temperature in the lower flux model during intrusive events. C) Empirical zircon U-Pb age CDF of the youngest 1.5 myr Puripicar zircons with thermal models that reasonably reproduce the observed distribution. D) Both models show prolonged melt presence. Intrusive episodes are buffered relatively well compared to the Chaxas Complex models, consistent with observations that magmatic reservoirs which produce supereruption scale dacites thermally and chemically buffer intrusions relatively efficiently.

Figure 8

Schematic diagram illustrating a generalized physical representation based on the temporal, thermal, geochemical, and modeled results of the Chaxas Volcanic Complex magmatic system. Upper surface of APMB from Pritchard et al. (2018). Depth range of pre-eruption storage estimated from PT conditions estimated for the APVC previously (Grocke et al., 2017; Lindsay et al., 2001). Pre-Chaxas shows run-up to 4.18 Ma Puripicar supereruption during high flux conditions that formed large volumes of monotonous dacite. Subsequent low flux magmatism from 3.54 – 1.24 Ma that characterized the Chaxas Complex depicts smaller discrete bodies of short lived melt within the Pre-Chaxas mush. Color gradient represents thermal gradient from the APMB. Surface volcanic features exaggerated for clarity.

Graphical abstract

Highlights

- Zircon petrochronology and thermal modeling applied to constrain flux and volume
- Flux varied 2 x 10^{-4} - 5.6 x 10^{-5} km^3 yr^{-1} km^{-2} (≤ 800 - 5800 km^3) within 200 kyr
- The preponderance of crustal magmatic assemblage occurs during stints of high flux
- Recycling of progenitor intrusions can be more efficient during high flux
- Zr/Hf ratios in zircon may track crustal assimilation

Two Stages of Volcanism at the Chaxas Volcanic Complex

Stage 1 5.44-3.73 Ma:
Large Volume (≥ 500 km^3) and Silicic Ignimbrite Eruptions

Stage 2 3.54 - 1.24 Ma:
Dome Forming (10 km^3) Eruptions

Approach

- LA-ICP-MS U-Pb Ages and Trace Elements
- Thermal Modeling of Ages

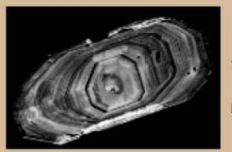

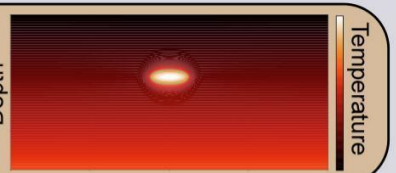

Results

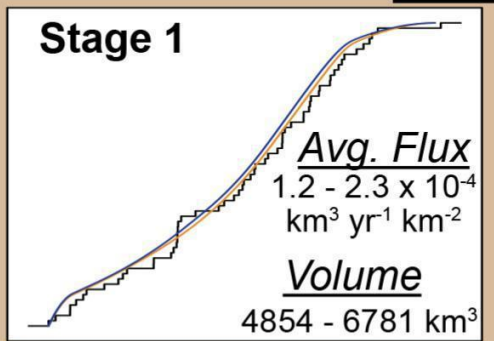

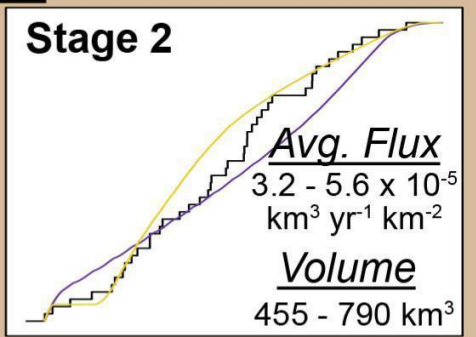

Questions

Did subvolcanic magmatic flux change between these two stages change? How quickly?

Conclusions

Flux into large volcanic systems can change by approximately an order of magnitude within 200 kyr. Pulses of flux may supply dominant intrusive volumes.

Graphics Abstract

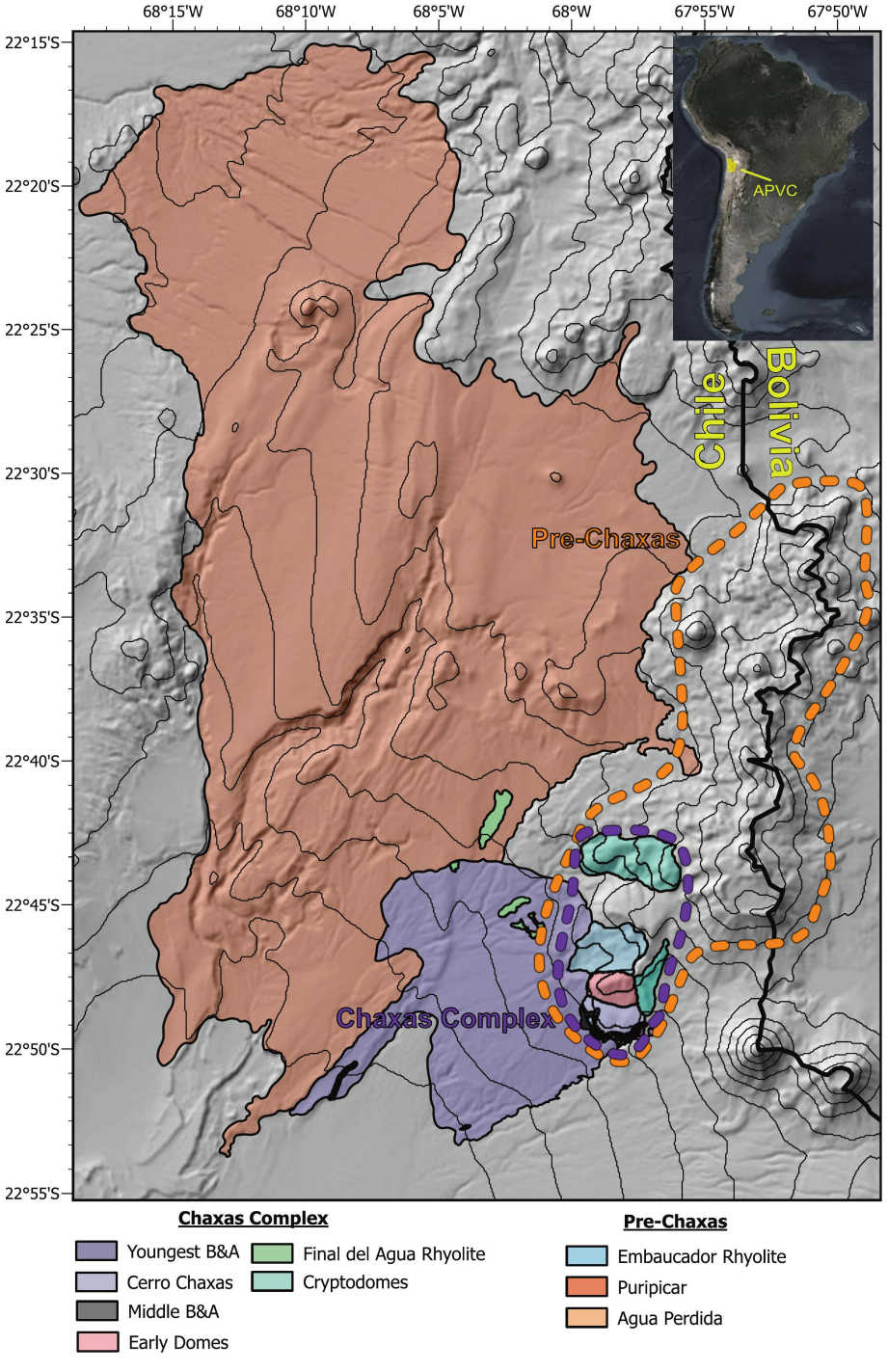
68°15'W
68°10'W
68°5'W
68°W
67°55'W
67°50'W
22°15'S
22°20'S
22°25'S
22°30'S
22°35'S
22°40'S
22°45'S
22°50'S
22°55'S
APVC
Chile
Bolivia
Pre-Chaxas
Chaxas Complex
Chaxas Complex
Youngest B&A
Cerro Chaxas
Middle B&A
Early Domes
Final del Agua Rhyolite
Cryptodomes
Pre-Chaxas
Embaucador Rhyolite
Puripicar
Agua Perdida

Figure 1

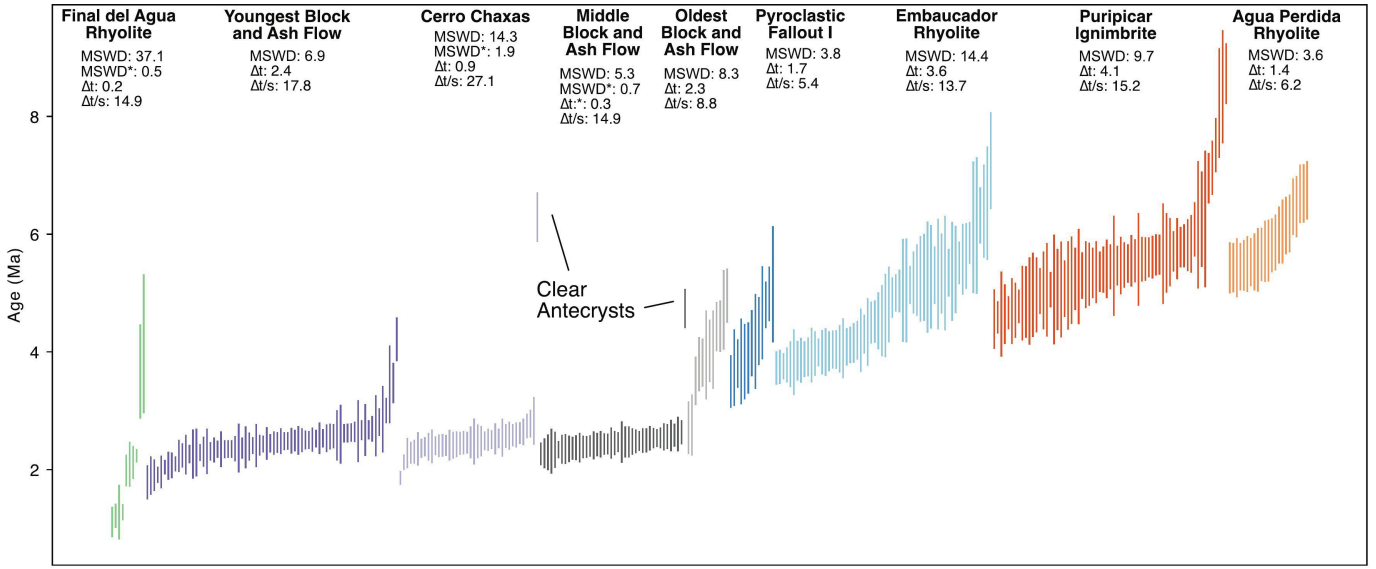
Final del Agua Rhyolite
MSWD: 37.1
MSWD*: 0.5
Δt: 0.2
Δt/s: 14.9
Youngest Block and Ash Flow
MSWD: 6.9
Δt: 2.4
Δt/s: 17.8
Cerro Chaxas
MSWD: 14.3
MSWD*: 1.9
Δt: 0.9
Δt/s: 27.1
Middle Block and Ash Flow
MSWD: 5.3
MSWD*: 0.7
Δt:*: 0.3
Δt/s: 14.9
Oldest Block and Ash Flow
MSWD: 8.3
Δt: 2.3
Δt/s: 8.8
Pyroclastic Fallout I
MSWD: 3.8
Δt: 1.7
Δt/s: 5.4
Embaucador Rhyolite
MSWD: 14.4
Δt: 3.6
Δt/s: 13.7
Puripicar Ignimbrite
MSWD: 9.7
Δt: 4.1
Δt/s: 15.2
Agua Perdida Rhyolite
MSWD: 3.6
Δt: 1.4
Δt/s: 6.2
Clear Antecrysts
Age (Ma)
8
6
4
2

Figure 2

Pre-Chaxas

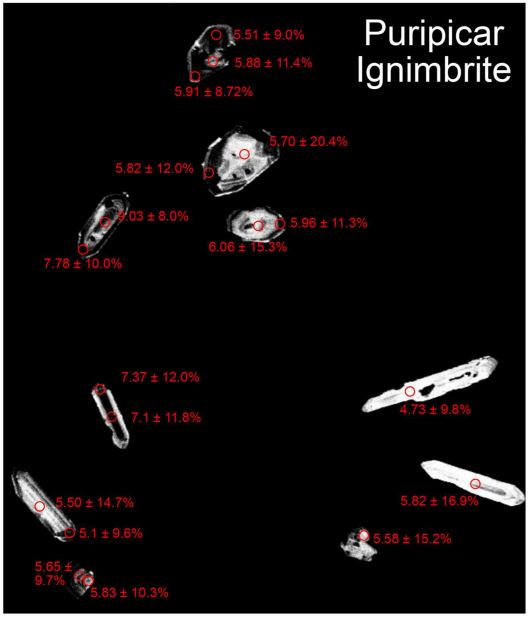

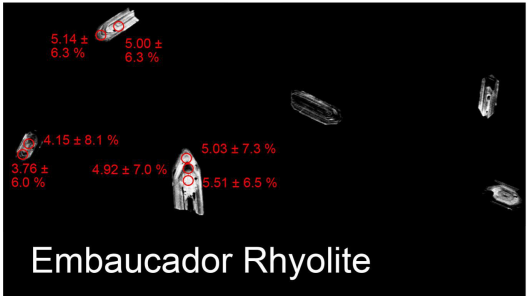

Chaxas Complex

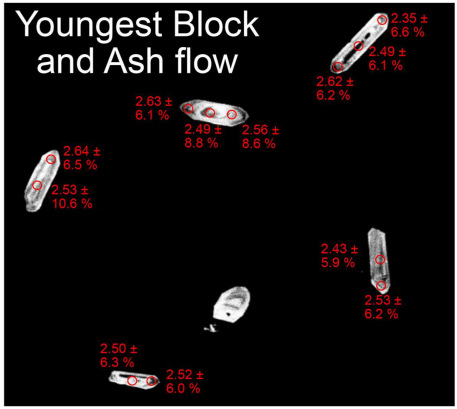

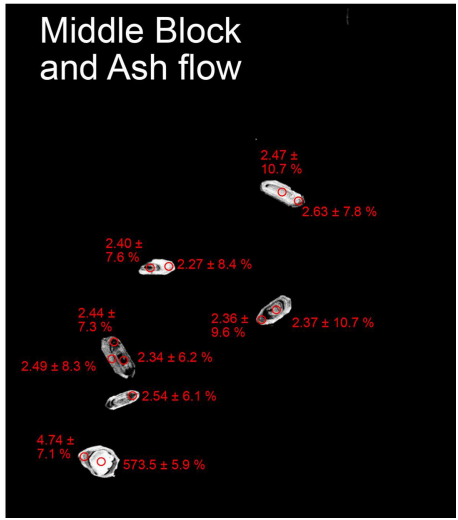

Figure 3

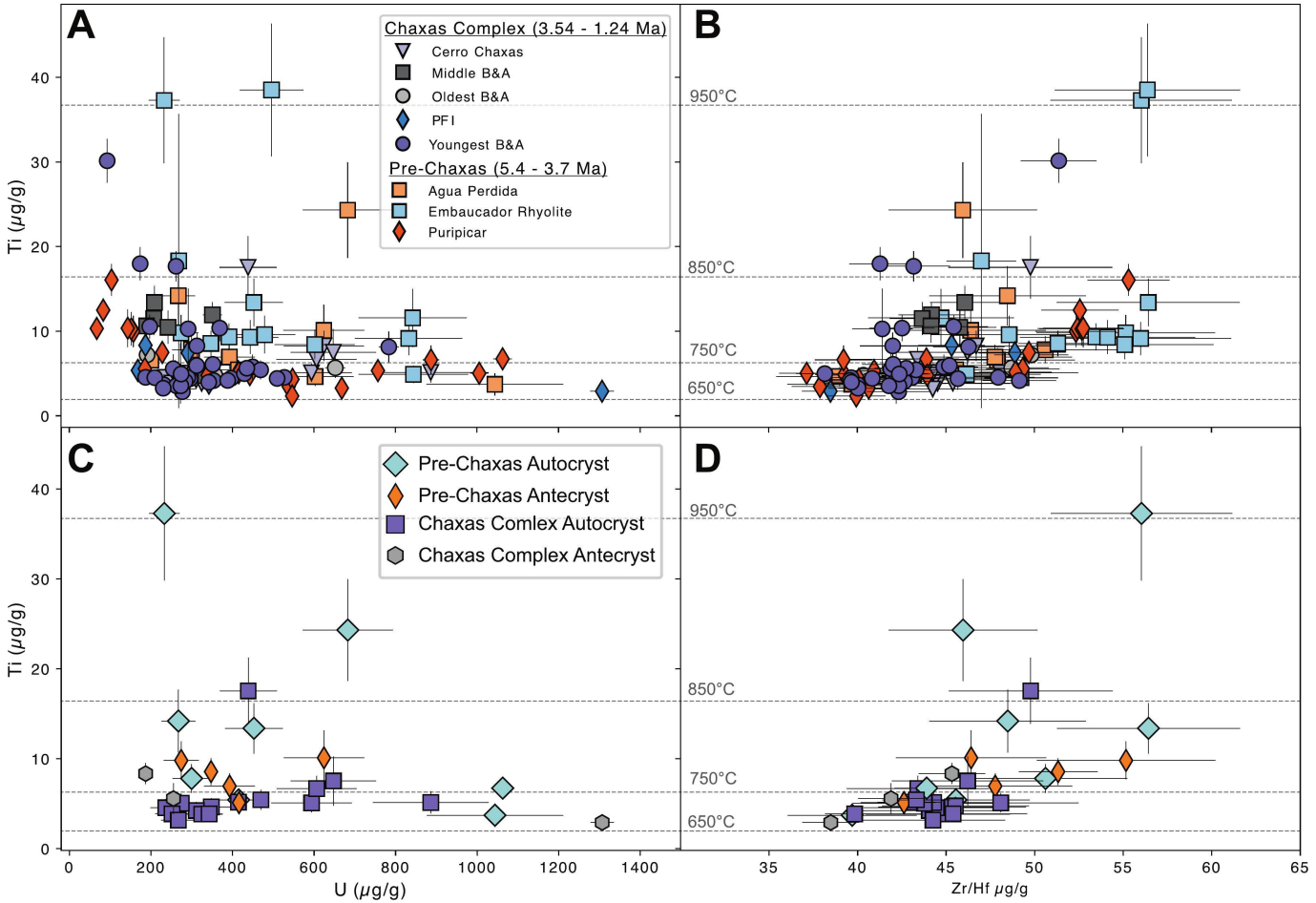
A
Chaxas Complex (3.54 - 1.24 Ma)
Cerro Chaxas
Middle B&A
Oldest B&A
PFI
Youngest B&A
Pre-Chaxas (5.4 - 3.7 Ma)
Agua Perdida
Embaucador Rhyolite
Puripicar
B
950°C
850°C
750°C
650°C
C
Pre-Chaxas Autocryst
Pre-Chaxas Antecryst
Chaxas Comlex Autocryst
Chaxas Complex Antecryst
D
950°C
850°C
750°C
650°C
Ti (μg/g)
Ti (μg/g)
U (μg/g)
Zr/Hf μg/g

Figure 4

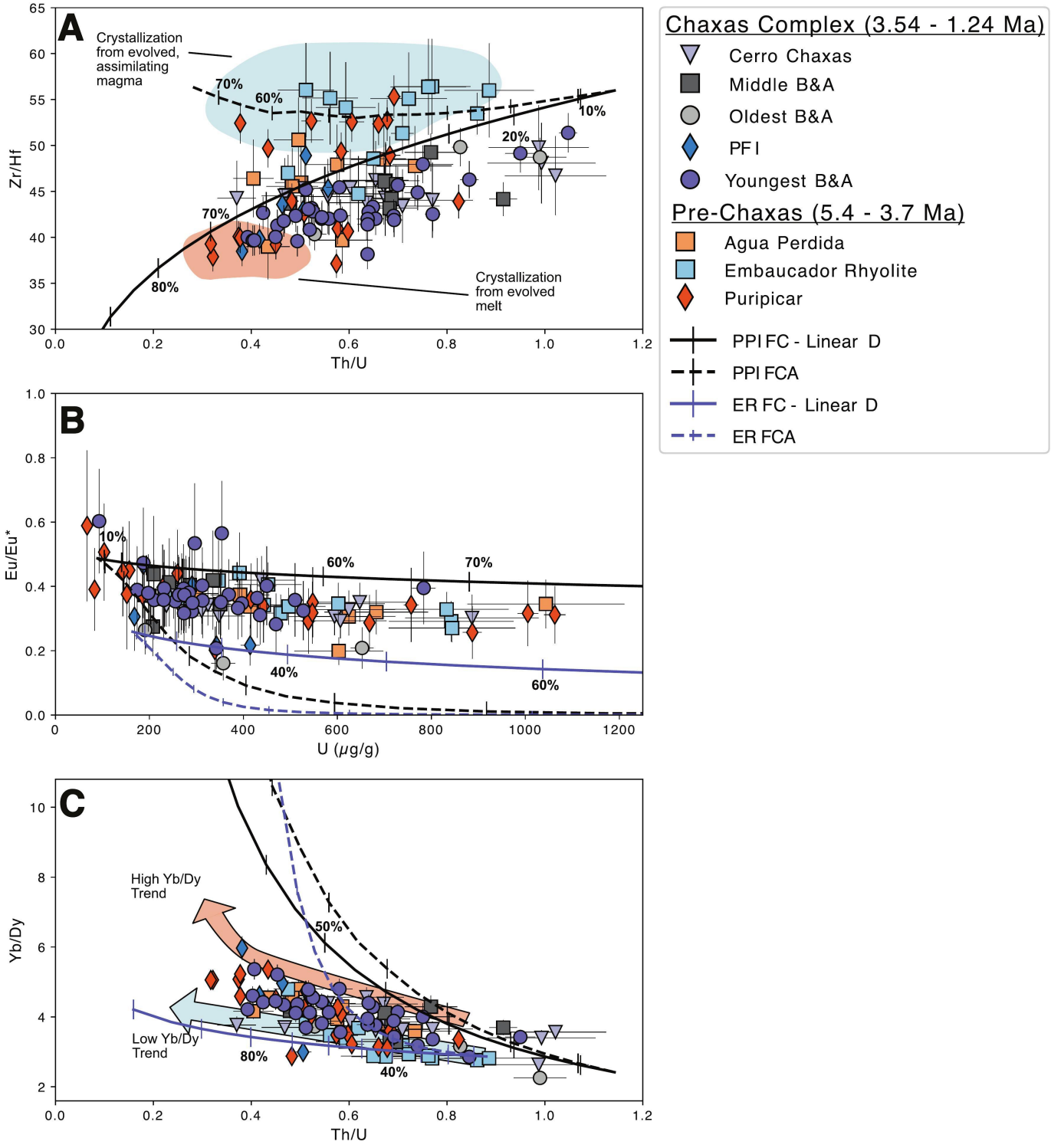
A
Crystallization from evolved, assimilating magma
70%
60%
10%
20%
70%
80%
Crystallization from evolved melt
Zr/Hf
Th/U
B
10%
60%
70%
40%
60%
Eu/Eu*
U (μg/g)
C
High Yb/Dy Trend
50%
Low Yb/Dy Trend
80%
40%
Yb/Dy
Th/U
Chaxas Complex (3.54 - 1.24 Ma)
Cerro Chaxas
Middle B&A
Oldest B&A
PFI
Youngest B&A
Pre-Chaxas (5.4 - 3.7 Ma)
Agua Perdida
Embaucador Rhyolite
Puripicar
PPI FC - Linear D
PPI FCA
ER FC - Linear D
ER FCA

Figure 5

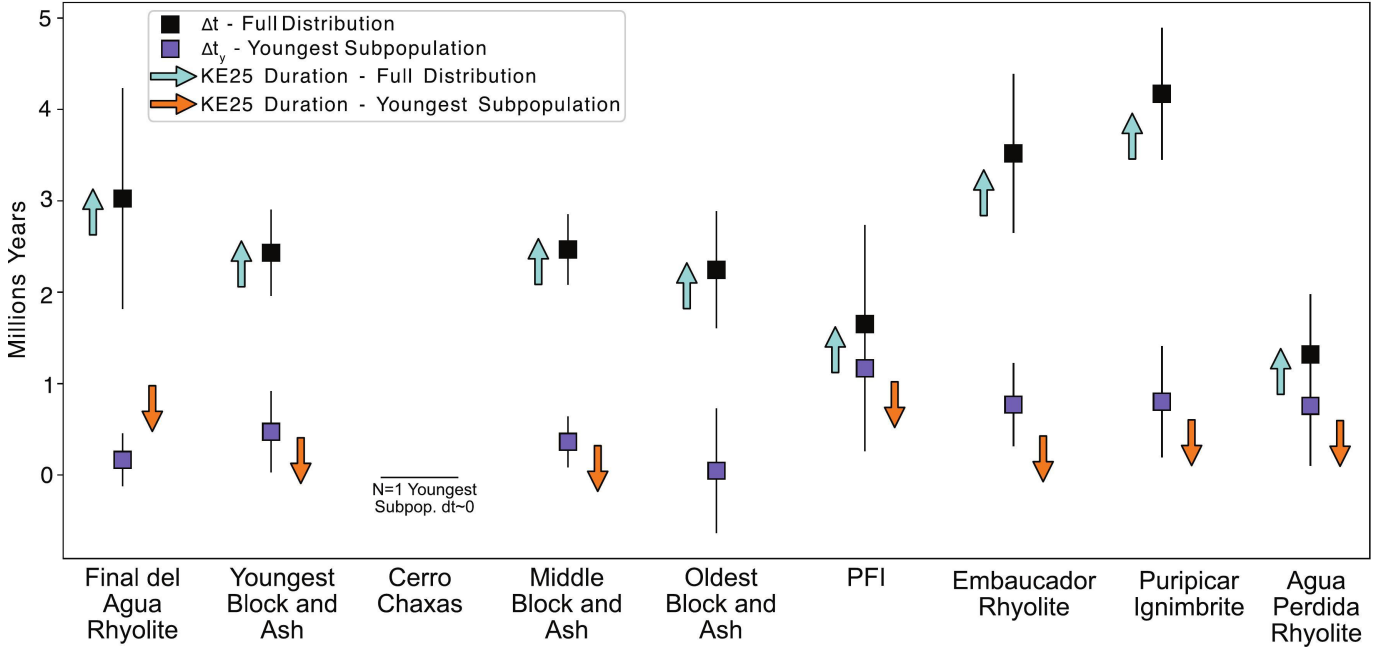
Δt - Full Distribution
Δt$_y$ - Youngest Subpopulation
KE25 Duration - Full Distribution
KE25 Duration - Youngest Subpopulation
Millions Years
5
4
3
2
1
0
N=1 Youngest Subpop. dt~0
Final del Agua Rhyolite
Youngest Block and Ash
Cerro Chaxas
Middle Block and Ash
Oldest Block and Ash
PFI
Embaucador Rhyolite
Puripicar Ignimbrite
Agua Perdida Rhyolite

Figure 6

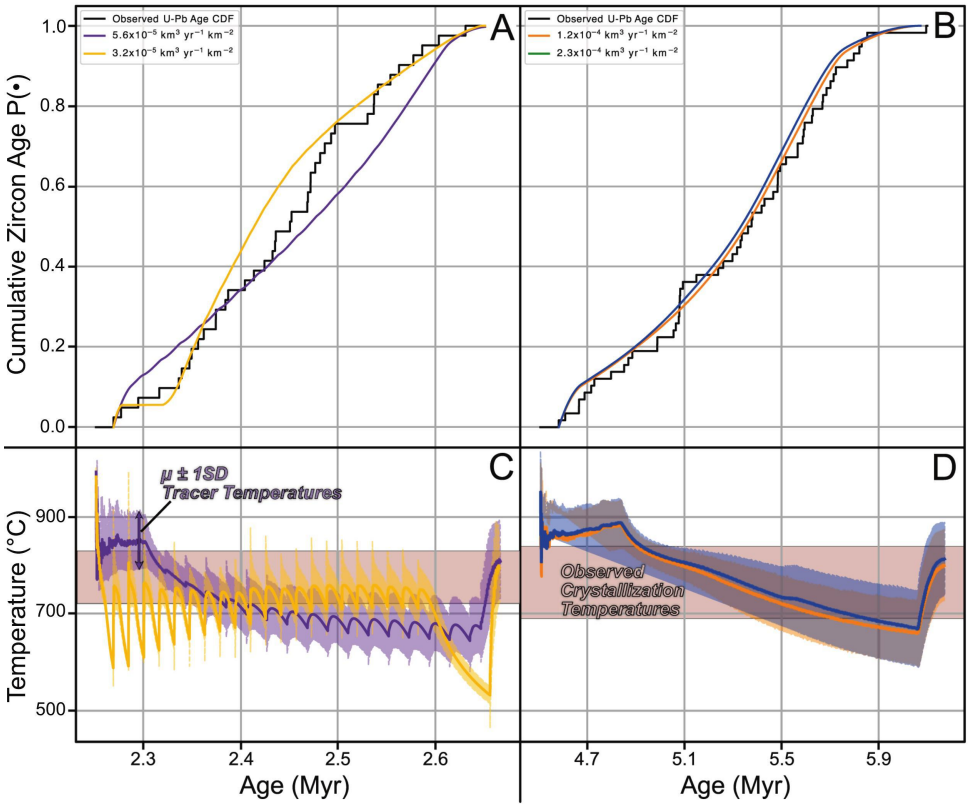
Chaxas Complex
Pre-Chaxas
A
B
C
D
Observed U-Pb Age CDF
5.6x10⁻⁵ km³ yr⁻¹ km⁻²
3.2x10⁻⁵ km³ yr⁻¹ km⁻²
Observed U-Pb Age CDF
1.2x10⁻⁴ km³ yr⁻¹ km⁻²
2.3x10⁻⁴ km³ yr⁻¹ km⁻²
Cumulative Zircon Age P(•)
1.0
0.8
0.6
0.4
0.2
0.0
μ ± 1SD
Tracer Temperatures
Observed
Crystallization
Temperatures
Temperature (°C)
900
700
500
2.3
2.4
2.5
2.6
Age (Myr)
4.7
5.1
5.5
5.9
Age (Myr)

Figure 7

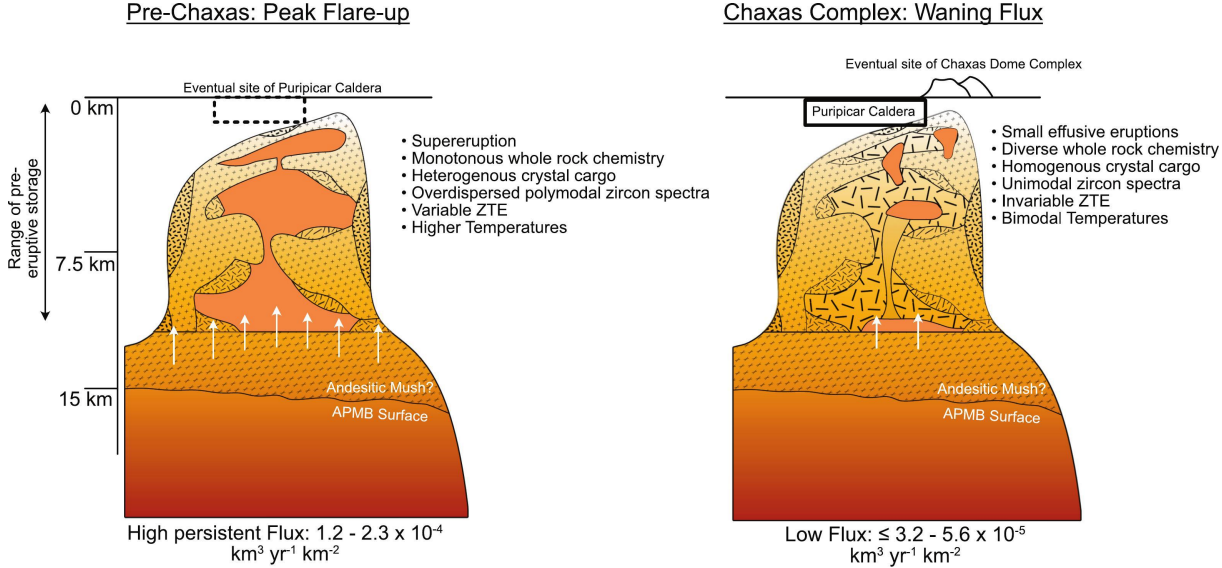
Pre-Chaxas: Peak Flare-up
Eventual site of Puripicar Caldera
0 km
7.5 km
15 km
Range of pre-eruptive storage
• Supereruption
• Monotonous whole rock chemistry
• Heterogenous crystal cargo
• Overdispersed polymodal zircon spectra
• Variable ZTE
• Higher Temperatures
Andesitic Mush?
APMB Surface
High persistent Flux: 1.2 - 2.3 x 10-4
km3 yr-1 km-2
Chaxas Complex: Waning Flux
Eventual site of Chaxas Dome Complex
Puripicar Caldera
• Small effusive eruptions
• Diverse whole rock chemistry
• Homogenous crystal cargo
• Unimodal zircon spectra
• Invariable ZTE
• Bimodal Temperatures
Andesitic Mush?
APMB Surface
Low Flux: ≤ 3.2 - 5.6 x 10-5
km3 yr-1 km-2

Figure 8